Nuclear Magnetic Resonance Cryoporometry

J. Mitchell [a], J. Beau W. Webber [b,c,d] J.H. Strange [c].

[a] *Department of Chemical Engineering, University of Cambridge, Pembroke Street, Cambridge, CB2 3RA, UK*

[b] *Institute of Petroleum Engineering, Heriot Watt, Edinburgh EH14 4AS, UK*

[c] *School of Physical Sciences, University of Kent, CT2 7NH, UK*

[d] *Lab-Tools Ltd., Canterbury Enterprise Hub, University of Kent, CT2 7NJ, UK*

Abstract

Nuclear Magnetic Resonance (NMR) cryoporometry is a technique for non-destructively determining pore size distributions in porous media through the observation of the depressed melting point of a confined liquid. It is suitable for measuring pore diameters in the range 2 nm – 1 μm, depending on the absorbate. Whilst NMR cryoporometry is a pertabative measurement, the results are independent of spin interactions at the pore surface and so can offer direct measurements of pore volume as a function of pore diameter. Pore size distributions obtained with NMR cryoporometry have been shown to compare favourably with those from other methods such as gas adsorption, DSC thermoporosimetry, and SANS. The applications of NMR cryoporometry include studies of silica gels, bones, cements, rocks and many other porous materials. It is also possible to adapt the basic experiment to provide structural resolution in spatially dependent pore size distributions, or behavioural information about the confined liquid.

Key words: NMR, cryoporometry, pore size distributions, Gibbs-Thomson equation
PACS: 64.60.-i, 81.07.-b, 61.18.Fs, 03.75.Hh, 05.70.Fh, 64.60.Qb, 64.70.Dv, 68.03.Cd, 68.08.-p, 82.56.Na, 82.56.Ub, 61.43.Gt, 61.46.+w, 82.60.Qr

Email address: jm600@cam.ac.uk, +44(0)1223 761631 (J. Mitchell).

Contents

1 Introduction

Porous materials have a multitude of roles in the natural world and are widely used in industrial applications. They exist in a vast range of forms: everything from biological cells to rocks, drying agents to catalysts in chemical reactors. It is important in many applications to be able to accurately characterise the properties of these systems, such as total porosity, pore size distribution, specific surface area, permeability, breakthrough capillary pressure, and radial density function. It can also be important to characterise the behaviour of liquids within porous systems by identifying diffusion and pore surface interactions.

Numerous methods currently exist for determining these properties, although each individual method can usually probe only one or two characteristics. These techniques range from the simplistic, such as crushing, imbibition, and microscopy (optical or electron), to the most complex Small-Angle Neutron Scattering (SANS) measurements requiring the use of a particle accelerator or nuclear reactor. Pore size distributions can be obtained using gas adsorption (usually with nitrogen) (Brunauer et al., 1938; Barrett et al., 1951), Differential Scanning Calorimetry (DSC) thermoporosimetry (Brun et al., 1977), Mercury Intrusion Porosimetry (MIP) (Ritter and Drake, 1945), SANS (Feigin and Svergun, 1987), and various Nuclear Magnetic Resonance (NMR) techniques (Watson and Chang, 1997; Barrie, 2000). Some of these methods, notably gas adsorption, DSC thermoporosimetry, and most NMR measurements, probe the surface-to-volume (S/V) ratio of the pore structure and assumptions have to be made about the pore geometry to derive a characteristic length scale (radius or diameter) for the porous matrix.

The most commonly used methods for determining pore size distributions are gas adsorption and MIP. These produce differing distributions as mercury intrusion measurements tend to probe the diameter of pore throats rather than the pores themselves. Often non-destructive testing is preferred and mercury intrusion fails in this regard, the measurement process damaging the pore matrix and making it impossible to reuse the sample. Here gas adsorption, NMR, and DSC methods all have an immediate advantage in that the samples remain undamaged so can be measured again and recovered. All three methods rely on placing a liquid in the pores, and the measuring the change in the thermodynamic properties caused by the resultant nano-structuring. Gas adsorption relies on the Kelvin relationship, concerning the change in the vapour pressure caused by this effect. Both NMR cryoporometry (Strange et al., 1993) and DSC thermoporosimetry rely on the Gibbs-Thomson equation concerning the relationship between the characteristic pore length scale and the change in the freezing point of the liquid, or melting point of its solid crystal, due to confinement within the porous matrix (see section 2). However, the freez-

ing and melting behaviour of confined liquids / solids is often complex, with the thermodynamic properties of the confined material being modified from those of the bulk (Christenson, 2001; Overloop and van Gerven, 1993). NMR cryoporometry has an advantage over DSC thermoporosimetry in that DSC measures transient heat flows and thus has a minimum rate at which the measurement may be made. The NMR method returns an absolute signal that may be measured arbitrarily slowly, or in discrete steps, to obtain improved resolution or signal-to-noise (S/N) ratio. In terms of accuracy of results, all the methods require interpretation and assumptions leading to possible systematic errors. NMR cryoporometry offers the advantage of a more direct measure of the open pore volume.

2 Theory

2.1 Thermodynamics: development of the Gibbs-Thomson equation

J. W. Gibbs, J. Thomson, W. Thomson (later Lord Kelvin), and J. J. Thomson were the pioneers of the theory behind phase transitions for confined materials. They employed thermodynamics, generalized dynamics, and experimentation to determine the effects that variables, including geometry, have on basic properties of matter such as vapour pressure and melting point (Gibbs, 1906 reprinted 1961, 1928; Thomson, 1849, 1862, 1871, 1888). In particular, they established that the shift in melting point for a small crystal relative to the bulk melting point varies inversely with crystal size (diameter). This behaviour is closely related to the capillary effect and both reflect the change in bulk free energy caused by the curvature of an interfacial surface under tension (Defay et al., 1951 reprinted 1966; Gregg and Sing, 1967). Consequently, the Gibbs-Thomson equation for the melting point depression, ΔT_m, for a small isolated spherical crystal, of diameter x, in its own liquid, may be expressed as

$$\Delta T_m = T_m^\infty - T_m(x) = \frac{4\sigma_{sl} T_m^\infty}{x \Delta H_f \rho_s}, \tag{1}$$

as given by Jackson and McKenna (Jackson and McKenna, 1990), where T_m^∞ is the bulk melting point of the solid (considered to be a crystal of infinite size); $T_m(x)$ is the melting point of crystals of diameter x; σ_{sl} is the surface energy at the crystal-liquid interface; ΔH_f is the bulk enthalpy of fusion (per gram of material); ρ_s is the density of the solid. ΔT_m depends only on the properties of the liquid, its solid, and the interfacial interaction between these two states.

The specific origins of the Gibbs-Thomson equation can be found in the works of J.J. Thomson who applied generalised dynamics to describe the effects of curvature on the equilibrium temperature of a liquid droplet surrounded by its own vapour (Thomson, 1888). By considering the mean Lagrangian function L of a gas, liquid, and solid, for the evaporation of a small droplet it is possible to show

$$RT \ln\left(\frac{P_0}{P_v}\right) + RT\left(\frac{\rho_v}{\rho_l}\right) + \psi\left(T\right) - \Delta H_0 + \frac{d\Delta L}{dm} = 0, \tag{2}$$

where R is the gas constant; T is the absolute temperature; P_0 is the ambient pressure; P_v is the vapour pressure; ρ_v and ρ_l are the vapour and liquid densities respectively, $\psi(T)$ is a function of temperature; ΔH_0 is the latent heat at absolute zero; m is the mass of liquid.

A change in mass m of a small droplet will change ΔL according to

$$\frac{d\Delta L}{dm} = \frac{2\sigma_{lv}}{R_k \rho_v} \tag{3}$$

where R_k is the Kelvin radius. From this is it possible to obtain, by substitution into eq. (2) under the condition of constant temperature, the Kelvin equation (Thomson, 1871, 1888)

$$RT \ln \frac{P_v}{P_0} = -2\gamma \frac{V_M}{R_k}, \tag{4}$$

where γ is the liquid surface tension at temperature T; V_M is the molar volume of the liquid.

The constant pressure variant of eq. (2) gives

$$\Delta T_m = \frac{T_m^\infty}{\Delta H_f} \frac{d\Delta L}{dm}. \tag{5}$$

Substituting in eq. (3) for a solid-liquid interface gives the Gibbs-Thomson equation (1) in the form

$$\Delta T_m = \frac{T_m^\infty}{\Delta H_f} \frac{2\sigma_{sl}}{R\rho_s}, \tag{6}$$

applicable to a crystal of radius R such that $x = 2R$.

The Kelvin equation (4) applies to an isolated droplet in its own vapour. This can further be applied to the model of a right cylindrical void containing a hemispherical interface between a completely wetting liquid and its own vapour (Thomson, 1888) as in the condensation branch of absorption isotherms (Gregg and Sing, 1967; Coelingh, 1938; Cohan, 1938). Analogously the Gibbs-Thomson equation applies to a spherical crystal in its own liquid, and by extension to a right cylindrical void containing a hemispherical interface between a non-wetting crystal and its own liquid.

The presence of a confining geometry requires additional terms to be incorporated into the Kelvin and Gibbs-Thomson equations to accommodate the interaction between the absorbate and the pore walls. Considering first the Kelvin equation (4), the Young equation (Defay et al., 1951 reprinted 1966; Gregg and Sing, 1967)

$$\sigma_{pv} = \sigma_{lv} \cos(\phi) + \sigma_{pl}, \tag{7}$$

indicates a $\cos(\phi)$ term should be present, where ϕ is the contact angle between the liquid and its own vapour; σ_{lv}, σ_{pv}, and σ_{pl} are the surface energies at the liquid-vapour, pore-vapour, and pore-liquid interfaces respectively. The Young-Dupré equation (Defay et al., 1951 reprinted 1966)

$$W_{pl} = \sigma_{lv} + \sigma_{pv} - \sigma_{pl}, \tag{8}$$

gives the reversible work necessary to separate unit area of the liquid from the pore wall. By simple substitution we can see

$$W_{pl} = \sigma_{lv} [1 + \cos(\phi)]. \tag{9}$$

Hence for a description of a liquid drop in a cylindrical pore the Kelvin equation becomes

$$RT \ln \frac{P_s}{P_0} = -2\gamma \frac{V_M}{R_k} \cos(\phi). \tag{10}$$

For the case of coexisting solid and liquid phases in a pore the analogous set of equations

$$\sigma_{pl} = \sigma_{sl} \cos(\phi) + \sigma_{ps}, \tag{11}$$

$$W_{ps} = \sigma_{sl} + \sigma_{pl} - \sigma_{ps}, \tag{12}$$

and

$$W_{ps} = \sigma_{sl} [1 + \cos(\phi)], \tag{13}$$

provide the reversible work required to separate unit area of the solid from the pore wall, where the surface energy terms σ_{pl} and σ_{ps} describe the pore-liquid and pore-solid interactions respectively. Thus for a generic crystal melting in a cylindrical pore the Gibbs-Thomson equation (1) becomes

$$\Delta T_m = T_m^{\infty} - T_m(x) = -\frac{4\sigma_{sl}T_m^{\infty}}{x\Delta H_f \rho_s}\cos(\phi). \tag{14}$$

The contact angle is commonly assumed to be 0^o in the liquid-vapour (Kelvin) case and 180^o in the solid-liquid (Gibbs–Thomson) case (Gregg and Sing, 1967; Jackson and McKenna, 1990; Young, 1805, 1855; Tell and Maris, 1983; Martin et al., 2002). The $\cos(\phi)$ term also has a straightforward geometric interpretation since a spherical meniscus of radius r_1, in a cylindrical capillary of radius r, with an angle of contact ϕ, has $r = r_1\cos(\phi)$ (Gregg and Sing, 1967).

In NMR cryoporometry experiments it is generally assumed most absorbates will have weak interactions with the absorbent surfaces, ensuring the pore dimension is the critical parameter defining the melting point depression. However, since

$$\cos(\phi) = \left(\frac{W_{ps}}{\sigma_{sl}} - 1\right), \tag{15}$$

it is clear that the contact angle will be dependent on the magnitudes of W_{ps} and σ_{sl}. Notably there is evidence that in some activated carbon fibres the melting point of the confined liquid actually increases (Watanabe et al., 1999), suggesting the $\cos(\phi)$ term has changed sign. This is discussed further in sections 7.2 and 8.1.2.

For convenience eq. (1) can be expressed in the form

$$\Delta T_m = \frac{k_{GT}}{x}, \tag{16}$$

where k_{GT} is a calibration constant to be determined empirically (Strange et al., 1993). It is important to be aware that eq. (14) applies unchanged only to right cylindrical pores, due to the numerical constant '4' being derived for this special case. In the general case, the influence of pore geometry must also be taken into consideration. It is therefore better to express eq. (16) in the form (Webber et al., 2007b)

$$\Delta T_m = \frac{k_{GT}}{x} = \frac{k_g \cdot k_s \cdot k_i}{x}, \tag{17}$$

where k_g is a geometric constant dependent on the interfacial shape (Webber, 2003a), k_s is a constant involving parameters specific to the crystalline solid of solid-liquid system employed such that $k_s = T_m^{\infty}/\Delta H_f \rho_s$, and k_i is an interfacial energy term such that $k_i = \sigma_{sl} - W_{ps}$ or $k_i = \sigma_{ps} - \sigma_{pl}$. Since the geometry of the pores is determined by the constant k_g, x becomes a generic "pore size" term as opposed to a more specific dimension such as radius R, diameter D, or slit separation T_{SS}. Nevertheless, in order to interpret the pore size distributions generated in NMR cryoporometry measurements, x is generally quoted as being a pore diameter unless evidence exists on the precise form of the pore geometry indicating x should be defined otherwise. The term k_g/x relates to the surface-to-volume (S/V) ratio of the porous matrix. In the case of a confined liquid freezing, it has been suggested that $k_g/x = S/V$ (Webber, 2003a; Petrov and Furo, 2006), whereas in the case of a confined crystal melting, it has been suggested that $k_g/x = \partial S/\partial V$(Petrov and Furo, 2006). However there is still some discussion regarding the exact nature of this relationship (Webber and Dore, 2008).

In real samples the geometry is often not perfect and so a precise value of k_g cannot be defined *a priori*; the pores may well be intersecting and could be of arbitrary or mixed geometries. Deviations from the thermodynamic ideal may also be expected for small dimensions where the molecular features of the confined phase are comparable with the pore size (Gelb et al., 1999; Sliwinska-Bartkowiak et al., 1999; Webber, 2000; Webber et al., 2001). This point is discussed further in section 7.

2.2 Thermodynamics: Application to NMR

NMR has been widely used for the study of the freezing and melting behaviour of water in pores. Overloop and van Gerven suggested that NMR was suitable for measuring gross pore volume, and for this application demonstrated the validity of the Kelvin Equation (although the Gibbs-Thomson form was quoted) (Overloop and van Gerven, 1993).

Strange *et al.* proposed a quantitative method, based on the Gibbs-Thomson equation, which they named "NMR cryoporometry" (Strange et al., 1993). This technique allowed the measurement of pore size distributions by differentiating and re-mapping the melting curve data using

$$\frac{\mathrm{d}v}{\mathrm{d}x} = \frac{k_{GT}}{x^2} \cdot \frac{\mathrm{d}v}{\mathrm{d}T}. \tag{18}$$

The acquired NMR cryoporometry data will contain a signal intensity proportional to the integral pore fluid volume, v, that will vary as a function of

temperature T. At any given temperature, v will be the volume of liquid in pores with a dimension less than or equal to x as given by eq. (16). After a small increase in temperature $\mathrm{d}T$, the total volume will increase by $\mathrm{d}v$ and will then represent a volume of liquid in pores with dimension less than or equal to $x + \mathrm{d}x$. The pore size distribution $\mathrm{d}v/\mathrm{d}x$ can be obtained from the slope of the curve of v against T (Strange et al., 1993).

NMR cryoporometry is a secondary method of measuring pore size distributions since the melting point depression constant, k_{GT}, of the absorbate must be initially calibrated using samples with known pore dimensions. Experimentally, to obtain a calibrated pore volume, it is only necessary to assume that the density of the absorbed liquid is independent of temperature (discussed further in section 4.3). It is possible, with care, to calibrate all the other factors in the NMR measurement to provide an accurate measure of the pore sizes.

Further studies of water in porous media revealed a hysteresis between the freezing (ΔT_f) and melting (ΔT_m) cycles of the confined liquid (Overloop and van Gerven, 1993). This hysteresis may be compared to the capillary condensation measured in gas adsorption (Beurroies et al., 2004). The non-equilibrium phase transition of a material freezing in a pore can be considered as a non-reversible process for small temperature fluctuations due to supercooling effects (Awschalom and Warnock, 1987). Therefore, melting curves have generally been used to determine pore size distributions, thus avoiding potential problems involving the supercooling of the liquid absorbate. Recently it has been shown that the true depressed freezing point can be readily determined if the excess (bulk) liquid in the sample is already in its solid phase, thus preventing nucleation-controlled freezing (Petrov and Furo, 2006; Webber et al., 2007a).

To conduct a NMR cryoporometry measurement only a simple modification to standard NMR apparatus is required: the inclusion of an accurate sample temperature control and measurement system. To determine a pore size distribution it is enough to record the intensity of the liquid signal as a function of temperature. High-resolution spectrometers additionally provide spectroscopic information on the absorbed liquid (Valiullin and Furo, 2002c), although accurate NMR cryoporometry measurements can be conducted using low-field permanent magnet (Strange et al., 1993) or electromagnet systems (Valckenborg et al., 2002). Such magnets can be advantageous in porous media studies since susceptibility induced field gradients at the solid / liquid interface that produce enhanced relaxation will be less significant at lower field strengths.

The majority of NMR cryoporometry experiments involve proton (^{1}H) NMR since an absorbate consisting of water or an organic substance is most easily measured. The observed magnetisation will be a measure of the number of proton spins in the liquid so if the liquid density remains constant, the signal will be proportional to the liquid volume. Three basic techniques are available to measure the signal intensity: the free induction decay (FID) (Bloch, 1946; Hahn, 1953), individual spin echoes (Hahn, 1956), or spin echo trains (Carr and Purcell, 1954; Meiboom and Gill, 1985). All these measurements are governed by the spin-spin, or transverse, relaxation time T_2, the time taken for spins to dephase in their local dipolar fields. In rigid solids T_2 is short (on the order of microseconds) whereas in liquids T_2 is much longer (ranging from milliseconds to seconds). The signal from the solid and liquid components should therefore be easily distinguishable. However some absorbates, such as cyclohexane, have a soft plastic crystal phase with a relatively long relaxation time and extra care must be taken to observe only the liquid signal (Booth and Strange, 1998). Cyclohexane has additionally been shown to have a complex phase diagram (Dore et al., 2004a), anomalous diffusion (Aksnes and Gjerdaker, 1999), and to exhibit critical scattering (Webber et al., 1996) when in confinement. There is also some evidence for the existence of metastable states (Dore et al., 2004a; Mu and Malhotra, 1992) although this has not been observed in NMR measurements due to problems associated with rapidly cooling the relatively large thermal mass of the samples. Further, there is now evidence (Awschalom and Warnock, 1987; Liu et al., 2006; Webber et al., 2007b) suggesting that, even for water, some of the ice formed in a pore may be in a plastic or rotationally mobile phase (Chezeau and Strange, 1979), with a T_2 longer than in normal brittle ice.

In a perfectly homogeneous magnetic field, as is approximated by high-resolution NMR spectrometer magnets, the FID (signal following a single radio frequency (RF) excitation pulse, normally giving a precession of 90^o) reveals the complete transverse relaxation directly. The integral intensity of the spectral peak (derived from the Fourier transform of the FID) corresponding to the liquid fraction of the sample is plotted as a function of temperature to generate the so-called $I(T)$ curve (Schmidt et al., 1995a).

However, in low-field permanent magnet systems, the FID will be dependent on magnetic field inhomogeneities. These cause the spins to dephase more rapidly than if they were in a homogeneous field. If ΔB_0 is the variation in the static magnetic field strength within the sample, the time constant of the FID signal will be strongly dependent on the spread in Larmor frequencies of the spins $\gamma_p \Delta B_0$ (where γ_p is the gyromagnetic ratio of the protons), provided that this time constant is less than the T_2 of the liquid in the pores. Since

we are concerned with liquids, this condition is likely to be satisfied and the measured relaxation time, denoted as T_2*, will be determined more by the spectrometer system than the sample. To overcome this problem a spin echo can be measured. By using a 90^o_x-τ-180^o_y-τ-echo pulse sequence (where τ is the pulse spacing; x and y are the RF pulse phases) the loss in coherence of the spins due to magnetic inhomogeneities can be overcome. The maximum height of the spin echo at time 2τ can be assumed to be proportional to the volume of liquid in the sample if τ is small compared to the transverse relaxation rate. By choosing an appropriate value of τ it is often possible to observe the liquid signal without any residual magnetisation from the frozen solid, even when the solid is a plastic crystal.

It is well known that the measured relaxation time of liquid in confined geometry will be related to the S/V ratio of the confining pores, thus:

$$\frac{1}{T_2^{obs}} = \frac{1}{T_2^{bulk}} + \frac{1}{T_2^{surf}} \cdot \frac{\varepsilon S}{V}, \tag{19}$$

where $1/T_2^{obs}$ is the observed relaxation rate, $1/T_2^{bulk}$ is the bulk liquid relaxation rate, $1/T_2^{surf}$ is the relaxation rate of molecules absorbed on the pore surface, and ε is the thickness of the temporarily adsorbed liquid surface layer. Normally $T_2^{bulk} \gg T_2^{surf}$, so the observed relaxation rate is directly proportional to the S/V ratio. If a distribution of pore sizes is present in the sample then a range of T_2 values can be expected. The full T_2 behaviour of the liquid can be obtained by measuring an echo train using the Carr-Purcell-Meiboom-Gill (CPMG) sequence (Meiboom and Gill, 1985): 90^o_x-τ-($180^o_{\pm y}$-τ-echo-τ-)$_n$, where n is the number of acquired echo windows. Only the even echo intensities are stored to provide a decay almost independent of imperfect RF pulses and diffusion for suitably short values of τ. The decays can be processed either using a multi-component fitting algorithm or using an inverse Laplace transform (Butler et al., 1981) to obtain a distribution of pore sizes at each temperature. The relaxation measurement will be influenced by pore surface interactions and so can be used to obtain additional information during the NMR cryoporometry experiment. Echo trains are also useful since they can be fitted with simple exponential functions to determine a more accurate signal intensity at time $\tau = 0$. This provides a liquid volume that is independent of relaxation rate variations as a function of temperature, even in complex multi-component systems.

3 Experimental

3.1 Sample Preparation

In a standard NMR cryoporometry measurement the dried samples are imbibed with liquid so as to just overfill the pores. The extra liquid provides the bulk melting point as a source of reference. Care must be taken when choosing an absorbate. Whilst a number of organic substances have suitable thermodynamic properties, those that sublime cannot be used in these experiments. Sublimation is revealed by a decrease of integral liquid volume during the NMR cryoporometry experiment. Ideally something should also be known of the interaction between absorbent and absorbate before the experiment is conducted. Water, for example, is suited to studying very small pore diameters (< 5 nm) whereas an organic substance may have to be used for hydrophobic samples.

It is good practice, where possible, to seal the imbibed sample in glass tubes under low pressure. This is important to prevent excessive evaporation of the absorbate, particularly when using volatile liquids. For relaxation measurements the liquid should be pumped (freeze, evacuate, thaw, repeat) to remove any dissolved oxygen since paramagnetic oxygen dissolved in the sample will limit the observed relaxation. In a basic NMR cryoporometry experiment however, this is not always advantageous as a reduced relaxation time allows the use of a shorter repetition delay without influencing the result. Under filled samples are made in the same way, with the exception that the pore volume and density of the sample has to be predetermined to allow the correct quantity of absorbate to be added. These samples are additionally left for a few days prior to measurement to allow the absorbate to distribute evenly throughout the porous matrix.

3.2 The NMR cryoporometry measurement

Initially the sample must be cooled to well below the depressed freezing point of the absorbate. This is to overcome any potential supercooling effects that would keep the absorbate in a liquid state even below the expected minimum freezing temperature. This cooling phase can be conducted *in-situ* inside the magnet and should be performed slowly to prevent the formation of metastable states. A warming run (melting) can be conducted immediately at this point. To conduct a porometric cooling run (freezing) the sample should be warmed to just below the bulk melting temperature so only the absorbate in the pores has thawed, and then cooled. In this manner the correct depressed freezing

point should be observed (Petrov and Furo, 2006). The NMR data can either be collected as the temperature is continually ramped in a 'scanning' experiment, or acquired at set temperature intervals in a 'stepped' experiment. Rapid acquisition techniques e.g. FID and single spin echoes are suited to the former method, whereas spin echo trains are better acquired using the latter method. NMR cryoporometry experiments can also be performed using absorbates with bulk melting points above ambient temperature (Strange et al., 2003). This makes the experiment easier to perform and less costly without requiring the use of cryogens.

Regardless of the acquisition technique, the NMR data will contain signal intensity as a function of temperature; see figure 1(a). On a warming run, the data should exhibit a pore melting step(s) and a bulk melting step. These steps may be separated by a constant volume plateau, depending on the range of pore sizes being measured and the k_{GT} constant of the absorbate. The signal intensity will be the total liquid volume in the sample at any given temperature and this must be differentiated to provide a pore size distribution, as shown in eq. (18); see figure 1(b). The temperature scale (x-axis) can be mapped onto a pore size scale using eq. (16). If the mass and density of the absorbate are known then the signal intensity (y-axis) can be converted into a calibrated pore volume.

3.3 Calibration

Before a new absorbate can be used in a NMR cryoporometry measurement its melting point depression constant k_{GT} must be determined in a set of calibration experiments. Mono-dispersed porous silica gels, with known median pore diameters determined by gas adsorption, make excellent calibration samples. Templated silicas with narrower pore distributions and relatively large median diameters can now be obtained such as MCM, SBA, and FSM (Webber et al., 2007a; Schmidt et al., 1995a; Anandan and Okazaki, 2005; Dore et al., 2004b; Akporiaye et al., 1994; Alba et al., 1996; Dosseh et al., 2003; Morishige and Kawano, 1999; Schmidt et al., 1995b; Xie et al., 2000). However, consideration must be given to the differing pore geometries.

The melting point depression constant k_{GT} has been determined, for example, for cyclohexane and water in a range of sol-gel silicas by plotting the average pore melting points against inverse median pore diameter determined from nitrogen gas adsorption. The melting points were recorded using a 20.8 MHz ^{1}H 'scanning' cryoporometer (Dore et al., 2004a). For cyclohexane the line of best fit gives $k_{GT} = 190.1$ K nm (Dore et al., 2004a); see figure 2(a). For water, $k_{GT} = 58.2$ K nm (Webber et al., 2001); see figure 2(b). Particularly note-worthy in this work is the high degree of co-linearity shown between

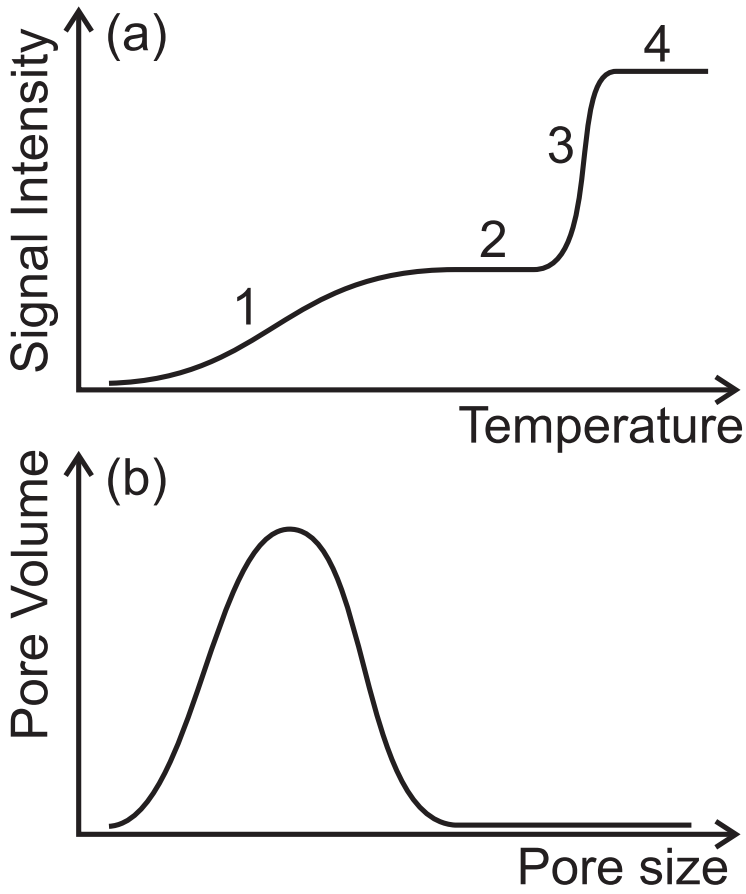

Fig. 1. (a) An ideal NMR cryoporometry melting curve with four main features: (1) pore melting step; (2) total pore volume plateau; (3) bulk melting step, and (4) total liquid volume plateau. (b) The pore distribution derived from the melting curve. Graphs reproduced with permission from Springer (Strange and Mitchell, 2006).

NMR cryoporometry and gas adsorption. In recent work, octamethylcyclotetrasiloxane was seen to have a larger melting point depression constant than cyclohexane, potentially allowing access to pores of greater than 1 μm diameter (Vargas-Florencia et al., 2007). Naphthalene, used for super-ambient NMR cryoporometry with a bulk melting point of $T_m^\infty = 354$ K, was determined to have a melting point depression constant of $k_{GT} = 181$ K nm by NMR and DSC measurements (Strange et al., 2003). Octaphenylcyclotetrasiloxane has also been suggested for high-temperature NMR cryoporometry ($T_m^\infty = 473$ K) although this has not yet been successfully demonstrated as a potential absorbate (Mitchell, 2003).

Careful analysis of the melting point depression data shows the best fit is obtained using $x - 2\varepsilon$ rather than just x, where ε is a surface layer of absorbate with modified molecular dynamics. The precise thickness of this layer appears to be temperature dependent (Webber et al., 2007a; Liu et al., 2006; Petrov et al., 2007). This surface layer was observed and studied for both water (Hansen et al., 1996b; Jehng et al., 1996; Pearson and Derbyshire, 1974)

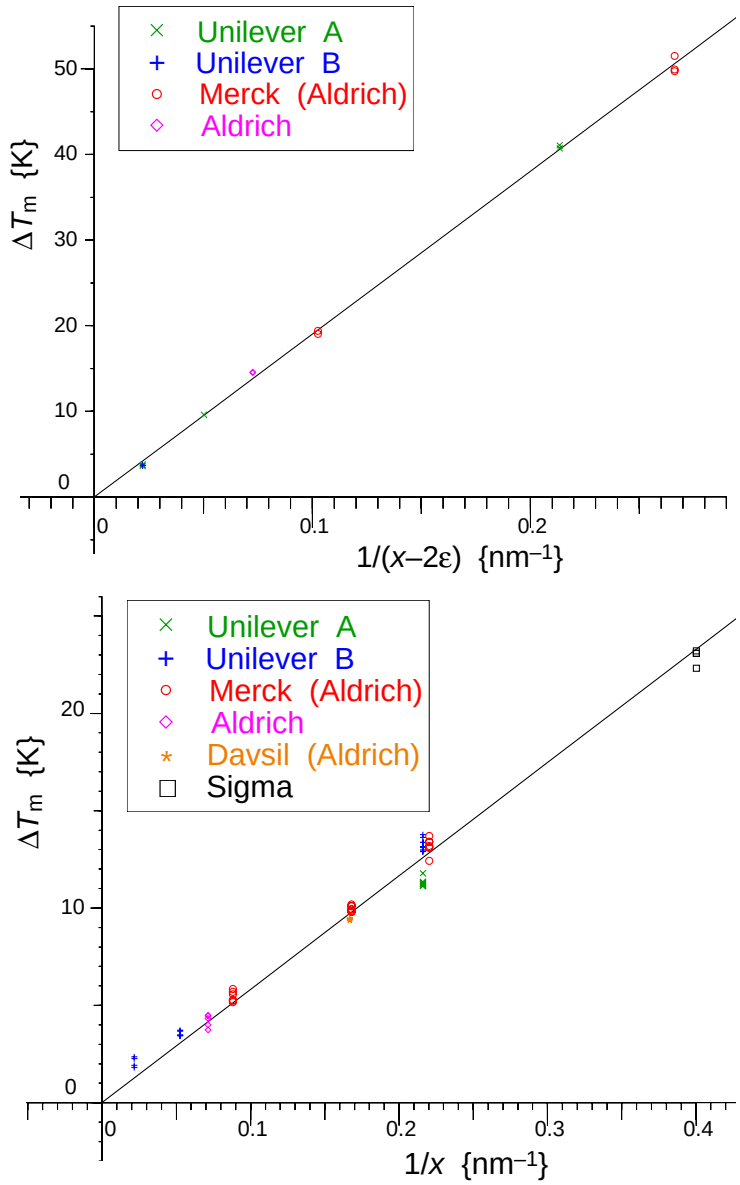

Fig. 2. (a) Measurement of melting point depression for cyclohexane in a series of sol-gel silicas from different manufacturers. The line of best fit gives k_{GT} = 190.1 K nm for an echo time 2τ = 20 ms, and assuming a surface layer of 0.12 nm. (b) Measurement of melting point depression of water in a series of sol-gel silicas from different manufactures. The line of best fit gives k_{GT} = 58.2 K nm for an echo time 2τ = 2 ms. In both graphs the calibration pore diameter was determined by nitrogen gas adsorption. Graphs reproduced with permission from Elsevier (Dore et al., 2004a,b).

and organic liquids (Webber, 2000; Hansen et al., 1996a). It was suggested by Stapf and Kimmich (Stapf and Kimmich, 1995) that the surface layer may interfere with the method of NMR cryoporometry by providing signal down to very low temperatures, thus being misinterpreted as indicating the presence of very small pores (Aksnes et al., 2001).

The surface layer was believed to consist of non-frozen material and some quasi-elastic neutron scattering data appeared to support such a view (Zanotti et al., 2005). In NMR cryoporometry measurements using a 'scanning' cryoporometer, ε for cyclohexane was determined to be slightly dependent on the value of the echo time 2τ (Webber, 2000; Strange et al., 2003). This unusual dependency is now believed to be a result of signal originating from the plastic nature of the cyclohexane crystal. More recent NMR relaxation and neutron diffraction cryoporometry evidence (Webber and Dore, 2008) has now been obtained (Webber et al., 2007a; Liu et al., 2006) suggesting that even for water, as the temperature is raised, a fraction of the brittle crystal converts initially not to liquid but to a plastic rotator-phase with a T_2 of 100 to 200 μs (Liu et al., 2006; Webber et al., 2007a,b). This lies between the T_2 of the brittle ice (10 μs) and that of the liquid in the pores (typically on the order of milliseconds). Valiullin and Furo used a magnetisation transfer experiment to further probe the surface layer of water frozen in porous glass (Valiullin and Furo, 2002b). By monitoring the transfer process the spin diffusion coefficient in ice was estimated. The magnetisation transfer experiment has also been applied to cyclohexane (Mitchell, 2003) and naphthalene (Mitchell and Strange, 2004) but with less success as only partial magnetisation transfer was observed.

The influence of the surface layer or a plastic crystal phase can be overcome by either using longer τ times in a single echo experiment or carefully fitting an echo train. More serious problems arise when the molecular size of the absorbate is a significant fraction of the pore diameter. It is then impossible for regular crystal lattices to form. Particularly in the case of organic absorbents, at low temperature, an amorphous or plastic state may be entered with properties similar to that of a glass. The smallest pore diameter that can be measured with cyclohexane is 3 – 4 nm (Mitchell, 2003). Naphthalene, having approximately twice the molecular radius of cyclohexane, can only be used to measure pore diameters greater than 6 nm (Mitchell and Strange, 2004). Water on the other hand, has been successfully used to measure pore diameters below 2 nm (Webber, 2000). Recent neutron scattering experiments in SPS-1 (Bagshaw and Hayman, 2001) indicated that under conditions of partial filling brittle crystalline ice does not form in pore sizes of around 1.5 nm; low density amorphous ice being found instead (Seyed-Yazdi et al., submitted, b).

4 Practical Considerations: Post Acquisition Corrections

4.1 Boltzmann Effect

Spin-½ protons have two energy levels due to Zeeman energy level splitting in a magnetic field. Since any two nuclei can be distinguished, we know from

Maxwell-Boltzmann statistics that the ratio of spins in the upper and lower energy states will be dependent on the absolute temperature T_K. The measured net magnetisation resulting from these variations in population levels will therefore also be temperature dependent. From the Curie Law we know this is approximately an inverse dependence and so the signal intensity, Si, can with good accuracy be corrected relative to the signal intensity at 0 ^{o}C (273 K) (Webber, 2000) thus:

$$\frac{Si\,(T_K)}{Si\,(273\text{ K})} = \frac{273}{T_K}. \tag{20}$$

This will also have an effect on the power of the excitation pulse required to fully saturate the sample. This is a minor effect in the measurement of liquids, whereas it can be significant when measuring solids. Ideally the power of the RF pulses should be constantly recalibrated, but this might not be necessary if the power is such that the pulses are short enough to provide sufficient bandwidth. Compared to the overall liquid signal amplitude this has a negligible effect and so can generally be ignored in NMR cryoporometry experiments.

4.2 NMR probe tuning

The receiver coil in the NMR probe will be temperature dependent due to changes in the thermodynamic properties of the wire. The signal amplitude will depend in part on the quality factor, Q, of the tuned circuit,

$$Q = \frac{\omega_0 L}{R}, \tag{21}$$

where ω_0 is the resonant frequency of the spins, L is the probe inductance, and R is the probe resistance. In the case of a probe with low Q, the excitation bandwidth will be large and there will be little need to adjust the circuit tuning during the course of the cryoporometry experiment. However if the Q is high then the shift in the resonant frequency of the circuit will result in a loss of signal. The resistance term in the LCR circuit is made up of the coil resistance, R_c, and other resistances, R_z, that are not temperature dependent. In the limit that $R_z/R_c\,(273\text{ K})$ is small, another approximately inverse correction can be applied, which can be expressed in Padé form (Webber, 2000)

$$\frac{Si\,(T_K)}{Si\,(273\text{ K})} = \frac{\alpha + \beta \cdot 273}{\alpha + \beta \cdot T_K}, \tag{22}$$

where α and β are thermal coefficients of the probe wire. Modern spectrometers now often include the ability to adjust the frequency of the transmitted / detected RF rapidly and automatically and this can be used to follow changes in the resonance condition as a function of temperature (Mitchell, 2003).

4.3 Density

The NMR signal is proportional to the number of resonant nuclei in the liquid. If the density of the liquid remains constant the signal is directly proportional to the pore volume. However, it is likely that thermal expansion / contraction will result in a change of density in the absorbate and the artificial confinement may moderate density changes unpredictably. Since the measurements are taking place below the bulk melting point of the liquids, bulk density information must be obtained from supercooling experiments (Bellissentfunel et al., 1986, 1989; Bosio et al., 1983; Takei et al., 2000). Information is also available from studying liquids in pores using SANS (Newport et al., 1988) and from the first diffraction peak using neutron or X-ray diffraction (Liu et al., 2006; Bosio et al., 1981; Dore, 2000; Seyed-Yazdi et al., submitted). Lacking further information it is generally assumed that the liquid density remains constant and thus the NMR signal is directly proportional to the liquid volume at all times.

4.4 Relaxation times

Liquids in porous media typically have complex relaxation behaviour governed by surface interactions. It can be difficult to reliably interpret NMR cryoporometry data generated from single echo intensities. This can lead to an unusual dependence of the melting point depression constant k_{GT} on the echo time 2τ (Strange et al., 2003) as discussed in section 3.3 Methods have been suggested to overcome the difference in the relaxation time between the pore and bulk liquids based on the acquisition of two spin echoes at any given temperature (Webber, 2000) for use in 'scanning' NMR cryoporometry measurements. Whilst such methods successfully remove single component relaxation time weighting, the complex relaxation behaviour often exhibited by liquids in porous media can only be successfully overcome by measuring either a FID in a homogeneous magnet or an echo train, both of which can be fitted to provide signal intensity that is almost independent of T_2 (Strange et al., 2003).

5 Hardware

An early NMR cryoporometry cooling system used the direct injection of liquid nitrogen into a 'splash-pot' constructed as part of the probe body and positioned close to the sample (the Lindacot system) (Norris and Strange, 1969). A heater placed in a Dewar forced droplets of liquid nitrogen into the probe. Thus the full latent heat of evaporation of the nitrogen was available to cool the probe and sample. The thermal mass of the 'splash-pot' smoothed out sudden temperature fluctuations due to the evaporation of individual liquid nitrogen droplets.

Most NMR system manufacturers now provide variable temperature probes for use in any magnet geometry. The majority of these systems operate using temperature regulated gas flow and this is suitable for achieving sub- and super-ambient sample temperatures. Dried, oxygen free nitrogen gas supply can be cooled in liquid nitrogen, or nitrogen gas can be boiled off directly from liquid in a Dewar. These cooling methods provide more uniform temperature changes than the Lindacot system although they do consume more liquid nitrogen. For super-ambient temperatures it is sufficient to simply heat an air flow. The temperature of the gas is stabilised and measured prior to being passed over the sample and it is assumed the sample temperature matches the gas temperature. A system now showing improved controllability utilises thermo-electric (Peltier) cooling / heating, and good results are being obtained from such a system (Webber, 2000; Webber et al., 2007a). Some examples of low-field variable temperature probe designs can be found elsewhere (Strange and Mitchell, 2006).

Accurately measuring the sample temperature is a fundamental problem in NMR cryoporometry. Ideally a thermocouple would be placed in direct thermal contact with the sample. Unfortunately this will conduct noise into the RF coil, thus ruining the measurement. Noise conduction can be overcome by electrically insulating and earthing the thermocouple, although this requires great care to be effective (Webber, 2000). An alternative method, not yet fully explored, is the use of an optical temperature sensor to remotely monitor the sample temperature. These sensors are limited in their ability to measure temperatures much below ambient, but as the technology improves this may become a viable alternative. Current optical thermometers would be suitable for super-ambient NMR cryoporometry measurements (Mitchell, 2003). Sensors optically monitoring the temperature dependent bandgap of a semiconductor (GaAs) (Roland et al., 2003) are also showing some promise and may provide the best alternative to thermocouples for direct sample temperature measurement.

6 Validation

Early NMR cryoporometry results (Strange et al., 1993) demonstrated the similarity of the measured pore volume distributions to those from the well-established nitrogen (gas) adsorption technique. The pore size distribution measured from a sample of 20 nm median diameter silica gel imbibed with cyclohexane can be seen in figure 3(a). This measurement was performed on a custom 14.3 MHz ^{1}H 'scanning' cryoporometer system. The ability to resolve multiple pore size ranges in a single sample was also demonstrated by producing a mixture of three silica gels with different median pore diameters. The measured melting curve, again obtained with cyclohexane as the absorbate, can be seen in figure 3(b). Figure 4 shows normalised pore size distributions for selected porous silicas: SBA-15, sol-gel, and Controlled Pore Glass (CPG) as measured by 'scanning' NMR cryoporometry at 20.8 MHz. The intrinsic resolution of the technique is better than the fully resolved SBA-15 silica pore size distribution with a median of 4.3 nm.

Good comparisons can be achieved on modern commercial systems without any significant modifications. The pore size distributions for a selection of silica gels measured using NMR cryoporometry (naphthalene; solid line) performed on a 23 MHz ^{1}H 'stepped' cryoporometer, DSC thermoporosimetry (cyclohexane; dotted line), and gas adsorption (nitrogen; +) are shown in figure 5. The NMR cryoporometry measurement suggests a lower median pore diameter and a broader distribution in the 20 nm silica, possibly due to the lower resolution of the 'stepped' measurement at larger pore sizes. In the 10 nm sample, the NMR and DSC data showed excellent agreement, although the gas adsorption suggested a higher median pore diameter. The NMR cryoporometry measurement indicated a significantly increased minimum pore diameter in the 6 nm silica sample due to the large non-frozen surface layer associated with the naphthalene preventing the smallest pores from being measured (Mitchell and Strange, 2004). Comparisons have also been made between NMR cryoporometry, MIP, and DSC thermoporosimetry in calcium carbonate structures (Gane et al., 2004).

NMR cryoporometry results have also been compared to pore size distributions obtained by SANS (Webber et al., 2001). A series of sol-gel silicas having median pore diameters ranging from 2.5 to 45.3 nm were studied using a 20.8 MHz ^{1}H 'scanning' NMR cryoporometry. Good agreement was seen between the two techniques at large pore sizes, but a deviation was observed for smaller pores ($x < 10$ nm). The authors associated this with a possible change in the liquid thermodynamic constants as atomic dimensions are approached, altering the co-linear gas adsorption and NMR cryoporometry calibrations. However, further NMR relaxation, neutron diffraction and SANS measurements on ordered MCM / SBA silicas indicate the presence of a plastic (rotational)

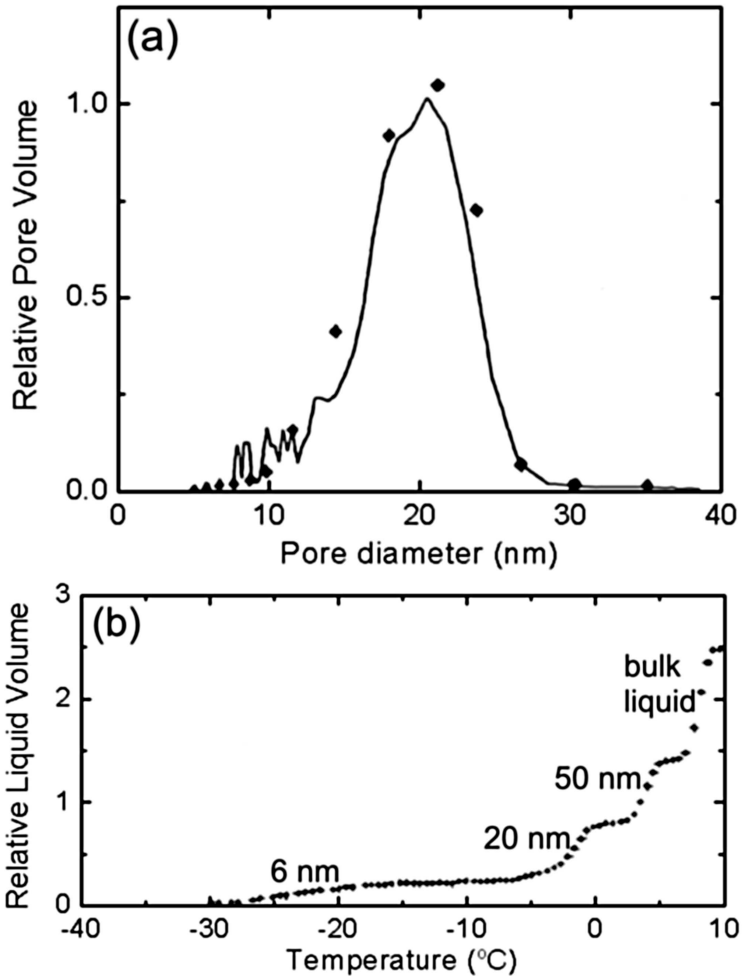

Fig. 3. (a) Pore size distribution for sol-gel silica with a median pore diameter of 20 nm. The solid line shows the NMR data, while the points (•) show the gas adsorption data.
(b) Melting curve measured from a sample containing silica gels with median pore diameters of 6, 20, and 50 nm. The absorbate was cyclohexane in both experiments. Graphs reproduced with permission from The American Physical Society (Strange et al., 1993).

phase of ice (Liu et al., 2006) that may possibly account for this divergence between the thermodynamic and scattering pore size distribution calibrations at small dimensions (Webber et al., 2001; Dore et al., 2004b).

Gun'ko *et al.* have recently suggested better agreement can be obtained between the pore size distribution obtained in NMR cryoporometry measurements and other methods, such as N_2 gas adsorption and thermally stimulated depolarisation current (TSDC) (Bucci and Fieschi, 1964) porosimetry, by inverting the integral form of the Gibbs-Thomson equation (Gun'ko et al., 2007b). However, this inherently forces the pore size distributions to a Gaussian shape, as in the method of using inverse Laplace transforms to interpret

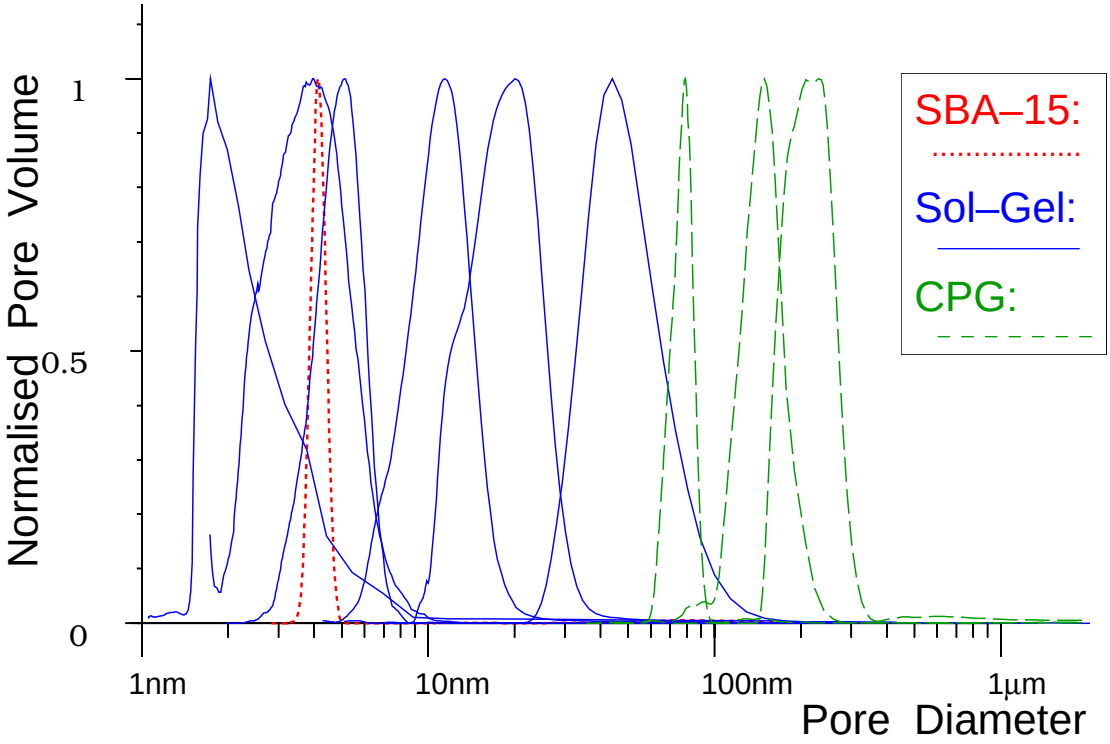

Fig. 4. Normalised pore size distributions for a selection of porous silicas measured using NMR cryoporometry: templated SBA-15 (Webber et al., 2007b), sol-gel (Webber, 2000; Dore et al., 2004b), and controlled pore glass (CPG) (Webber, 2000). The resolution of the measurements is such as to fully resolve even the narrow SBA-15 distribution. Graphs reproduced with permission from Lab-Tools Ltd.

NMR relaxometry data.

7 Advanced Techniques

7.1 Pore morphology

NMR cryoporometry can be used to obtain more information than simply the distribution of pore dimensions in the sample, particularly when combined with other techniques. Simply by combining NMR cryoporometry, density, and imbibation measurements, the solid (silica), pore, and inter-granular volumes and densities were accurately determined for a sol-gel silica sample (Webber et al., 2001). We have already discussed the prediction that the freezing point of a confined liquid may be related to the S/V ratio whereas the melting point may be related to the differential of the same. Petrov and Furo have suggested using the difference to obtain a measure of the integral mean curvature of the pores κ, since $\Delta T_{\mathrm{m}} \big/ \Delta T_{\mathrm{f}} = 2\kappa V/S$ (Petrov and Furo, 2006). By comparison with known geometries, it may be possible to deduce the pore

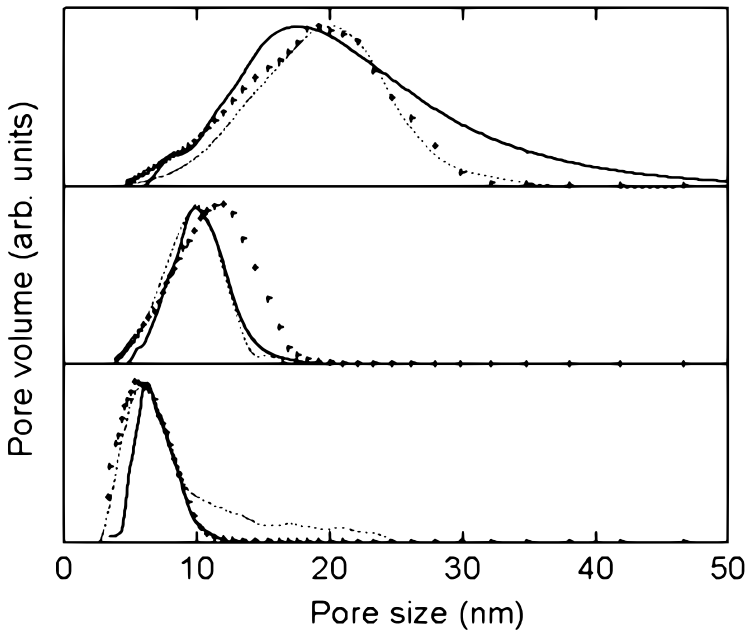

Fig. 5. Pore size distributions from silica gels with median pore diameters of 20 nm (top), 10 nm (middle), and 6 nm (bottom) measured using NMR cryoporometry with naphthalene as the absorbate (solid lines), DSC thermoporosimetry with cyclohexane as the absorbate (dotted lines), and nitrogen gas adsorption (+). Data previously presented elsewhere (Strange et al., 2003; Mitchell, 2003).

morphology.

The ability of NMR cryoporometry to probe pore morphology has been explored through the study of specially constructed porous silicon monoliths with intersecting channel-like pores of varying cross-section (Khokhlov et al., 2007). The presence of narrow pore throats was seen to retard homogeneous pore freezing in these structures.

It is possible to determine pore size by studying restricted molecular diffusion in a magnetic field gradient. This is the method of NMR diffusometry (Tanner and Stejskal, 1968; Callaghan, 1991). However, using reasonable field gradients, this technique can only probes pores on a much larger scale than those explored by NMR cryoporometry. The connectivity of pores can be explored by combining these measurements in a single experiment, called NMR cryodiffusometry (Filippov and Skirda, 2000; Filippov and Vartapetyan, 1997). By simultaneously observing the pore size distribution with NMR cryoporometry and the diffusion path lengths with NMR diffusometry, it is possible to determine the degree of connectivity within the porous structure as a function of pore size. NMR diffusometry can also be used to determine molecular diffusion in the liquid-like surface layer (Stapf and Kimmich, 1997) or on a pore surface by applying a monolayer coverage of liquid to a pore wall (Kärger et al., 2005; Valiullin et al., 2005).

Computer modelling techniques have been applied to simulate the behaviour of liquids in freezing in porous media (Dominguez et al., 1999) and the results have been shown to agree with experimentation (Radhakrishnan et al., 1999). Various pore geometries have been modeled such as cylinders (Maddox and Gubbins, 1997; Denoyel and Pellenq, 2002) and spheres (Brovchenko et al., 2000). The effects of ordered (Radhakrishnan et al., 2002b) and disordered (Coasne et al., 2006) pore structures have been explored, as well as the influence of excess bulk liquid (Brovchenko and Geiger, 2002). An improved model for simulating porous silica has been suggested by Hansen *et al.* (Hansen et al., 1997b). It has been shown through molecular dynamics simulations that the freezing and melting behaviour of simple confined liquids is additionally related to the surface tensions between the pore walls and the confined liquid / solid (Alba-Simionesco et al., 2006). There are many other variables in the Gibbs-Thomson equation preventing a direct measure of the surface interactions using the freezing / melting point depression alone. However, Gun'ko *et al.* have observed a variation in the chemical shift of water in the interfacial pore surface layers depending on the strengths of hydrogen bonding. A review has already been written on this subject (Gun'ko et al., 2005) covering studies of water in unmodified, modified, and partially modified fumed silicas, and also in biological systems (see section 8.5). Weakly associated interfacial water on hydrophobic surfaces was characterised by a chemical shift of $\sigma_H = 1.1 - 1.7$ ppm, whereas strongly associated water on hydrophilic surface exhibited a much larger chemical shift of $\sigma_H = 4 - 5$ ppm.

Sklari *et al.* studied the freezing of water in silica gels with varying surface acidity (Sklari et al., 2001). Whilst the pore freezing was seen to depend on the pore dimensions as expected, the surface layer of unfrozen water exhibited a continuous change in T_2 with decreasing temperature. The rate of change of T_2 with temperature was seen to depend on the surface acidity. A model was proposed describing the structure of the water in the mobile interfacial layer as a series of bridges between the acid sites on the silica.

The behaviour of interfacial water in silica containing adsorbed 1,3,5-trihydroxybenzene (phloroglucinol) has been studied with variable temperature NMR spectroscopy (Gun'ko et al., 2006a). Phloroglucinol acts as an ice-nucleator and so altered the structure of the confined water-ice. The spectral data indicated an increase in the thickness of the interfacial amorphous ice layer with increasing concentration of phloroglucinol. The amorphous nature of supercooled water and water-ice has been explored through simulations (Koga et al., 1998; Brovchenko and Oleinikova, 2006) and neutron diffraction experiments (Liu et al., 2006; Dore et al., 2002; Webber and Dore, 2004; Webber et al., 2007b; Webber and Dore, 2008; Seyed-Yazdi et al., submitted, b); see section 3.3 for additional discus-

sion and references.

Surface treatments of Ultra High Pore Volume (UHPV) silicas have been studied by low-field NMR cryoporometry (Strange et al., 2002); see figure 6. Water was used as the absorbent to probe the porosity of untreated silica (A), and silica treated with a hydrophilic surfactant (B) and a hydrophobic fluorine based surfactant (C). A shift in the smallest observable pore size in sample B was explained as a result of the smallest pores being completely filled by the surfactant. The median pore diameter was seen to reduce, suggesting the surfactant had coated the pores with a 2.5 nm surface layer. Almost no porosity was detected for sample C, although the authors noted that the hydrophobic surfactant probably prevented water imbibation. Sample C was successfully characterised by using cyclohexane as the absorbate and a similar surface coating thickness was calculated. The change in surface interaction was not seen to influence the NMR cryoporometry result, except for preventing water imbibition in sample C.

The spin interaction between the absorbent and the pore walls can be studied by a combined NMR cryoporometry and NMR relaxometry experiment (Valckenborg et al., 2002). Since the relaxometry measurement is sensitive to the enhanced relaxation of spins close to the pore wall (Brownstein and Tarr, 1979) the difference between the two measurements can be used to differentiate pore size and relaxation effects in NMR relaxometry. This technique was successfully used to demonstrate that sol-gel silicas from different manufacturers contain significantly varying quantities of paramagnetic impurities in the porous matrix (Mitchell et al., 2005); see figure 7. The NMR cryoporometry measurements, see figure 7(c), indicate the silicas have similar pore diameters whereas the NMR relaxometry suggested the pore size distributions differed significantly. The combined experiment showed more clearly how the relaxation measurement was dominated by the pore surface interaction.

The wetting of a pore surface has been explored as a means of determining the morphology through the study of partially saturated porous media. Combined with line-width studies of the same sample (Allen et al., 1997), NMR cryoporometry was used to determine the processes governing pore filling (Allen et al., 1998). A comparison was made between cyclohexane and water in porous silica; see figure 8 (a) and (b) respectively. At low saturation levels water was observed to form puddles on the surfaces of all the pores, characterised by dimensions smaller than the smallest pores in the sample. As the saturation levels increased, the puddles grew until a uniform coverage was achieved. Cyclohexane, in contrast, was seen to preferentially fill the smallest pores first. These different mechanisms were associated with the different surface interactions. Additional analysis incorporating magnetic susceptibility variations was suggested as a potential method of providing information on pore morphology (Allen et al., 2001).

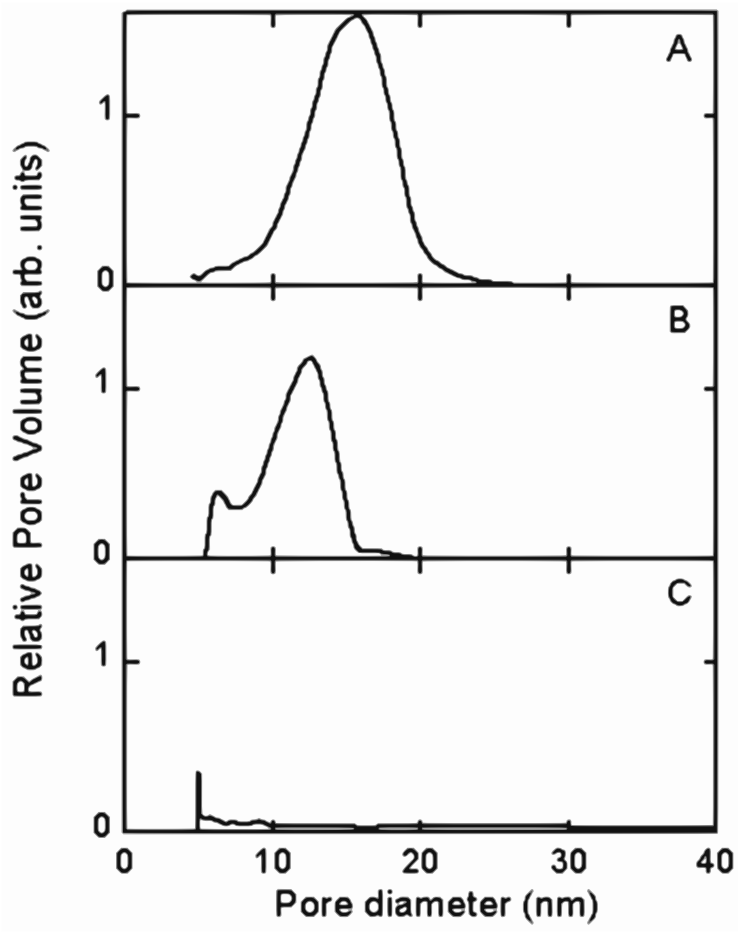

Fig. 6. NMR cryoporometry pore size distributions determined for water in three samples of UPHV silica. A: unmodified silica, median pore diameter 15 nm. B: silica modified with standard surfactant. C: silica modified with hydrophobic surfactant. Data previously presented elsewhere (Strange et al., 2002).

The strengths of surface interaction of two liquids can be compared indirectly using NMR cryoporometry by observing preferential pore filling. The preferential filling of small pores by water over decane was observed in porous sol-gel silica (Alnaimi et al., 2004) where the polar water molecules had a stronger surface interaction; see figure 9. The two absorbates were distinguishable in the melting curve due to their distinctly different melting points. As the fraction of water in the sample was increased, it could be seen that the decane was displaced from the smallest pores first. Additionally water was also observed to displace cyclohexane (Mitchell, 2003) and a miscible alkane mixture of heptadecane and decane was seen to separate in silica gels when the heptadecane absorbed preferentially (Mitchell et al., 2005). Valiullin and Furo also looked at binary mixtures of nitrobenzene and n-hexane in porous glass using NMR spectroscopy to resolve the two components (Valiullin and Furo, 2002c). They interpreted the results as droplets of nitrobenzene forming within a pore wetting layer of n-hexane. The droplet sizes were later investigated using pulsed

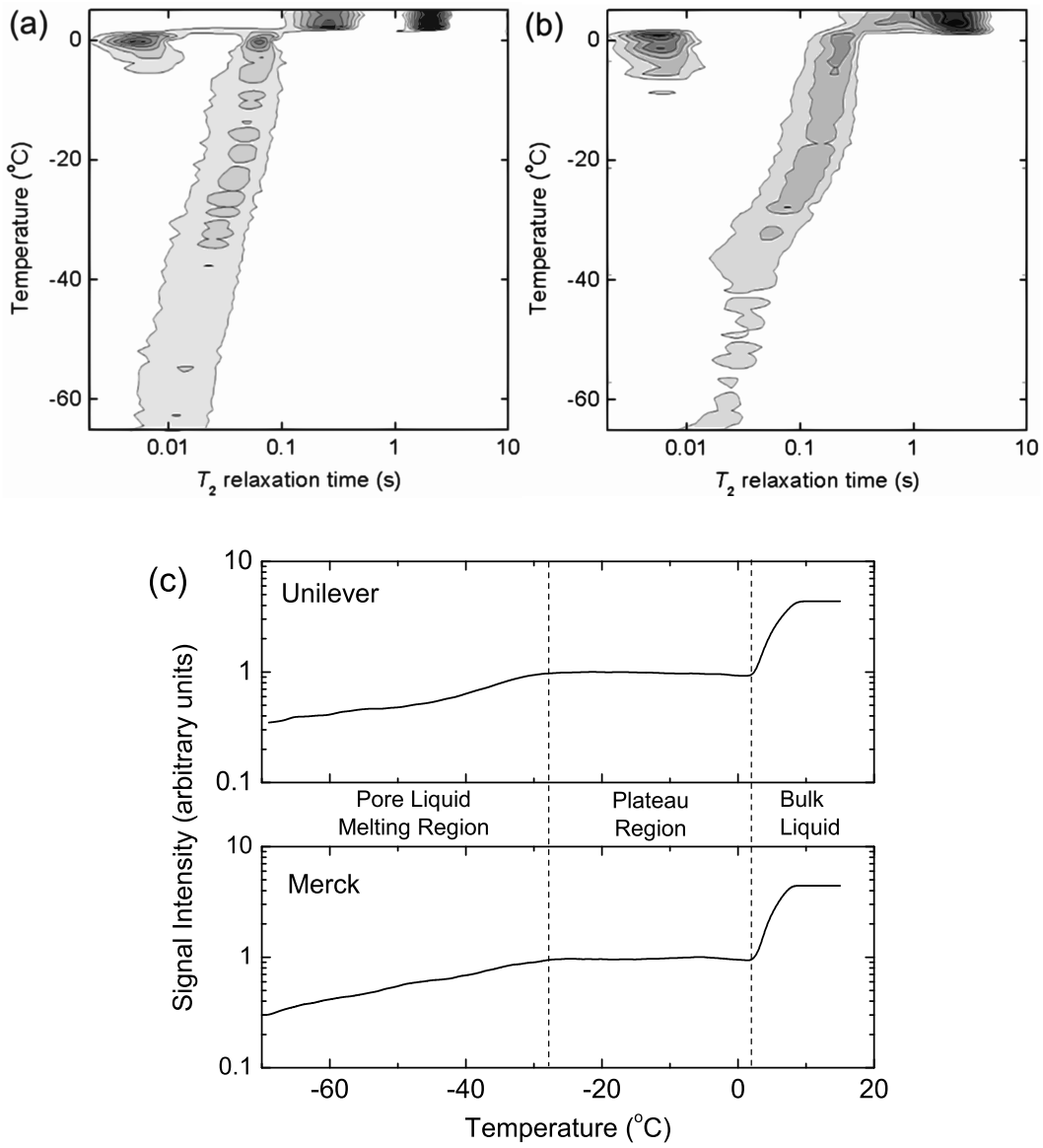

Fig. 7. Combined NMR relaxometry and NMR cryoporometry measurements for cyclohexane in 6 nm silica gel from two different manufacturers (a) and (b) respectively. The grey-scale ranges from white (no signal) to black (maximum signal) in both cases. The pore melting (vertical axis, repeated in (c) for clarity) is nearly identical for both samples, whereas the relaxation times (horizontal axis) are significantly different. Graphs reproduced with permission from the Institute of Physics (Mitchell et al., 2005).

field gradient techniques (Valiullin and Furo, 2002a).

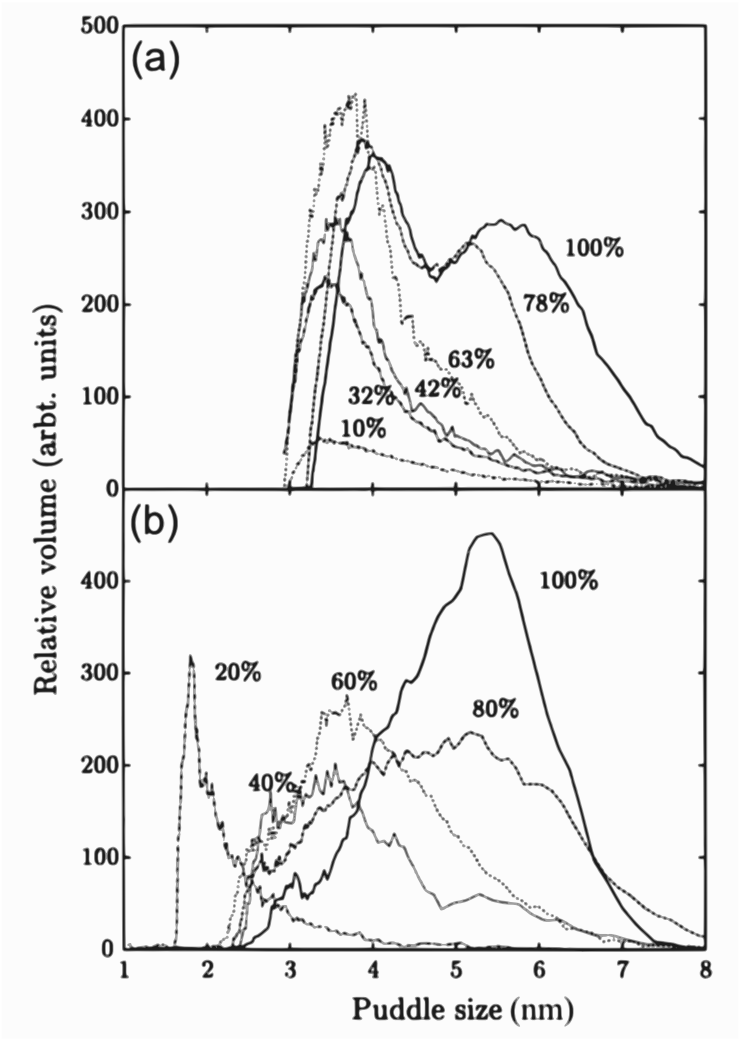

Fig. 8. Puddle size distributions for (a) cyclohexane and (b) water in 6 nm median pore diameter silica gel. Graphs reproduced with permission from the American Institute of Physics (Allen et al., 1998).

7.3 Spatially resolved pore size distributions

By constructing a variable temperature probe that fits inside a MRI scanner it is possible to obtain the spatial variation of the pore size distribution. Whilst the individual pores are too small to image, this combination of techniques allows the homogeneity of a sample to be explored. This method is particularly useful when studying materials such as cement where the conditions of manufacture may alter the distribution of pores across the sample. MRI theory will not be discussed here as there is already extensive literature covering this subject. However, it is worthwhile mentioning that NMR cryoporometry is perhaps most usefully combined with imaging techniques suitable for visualising short relaxation time materials such as stray field imaging (STRAFI) (Samoilenko et al., 1988) or single point imaging (SPI) (Emid and Creyghton,

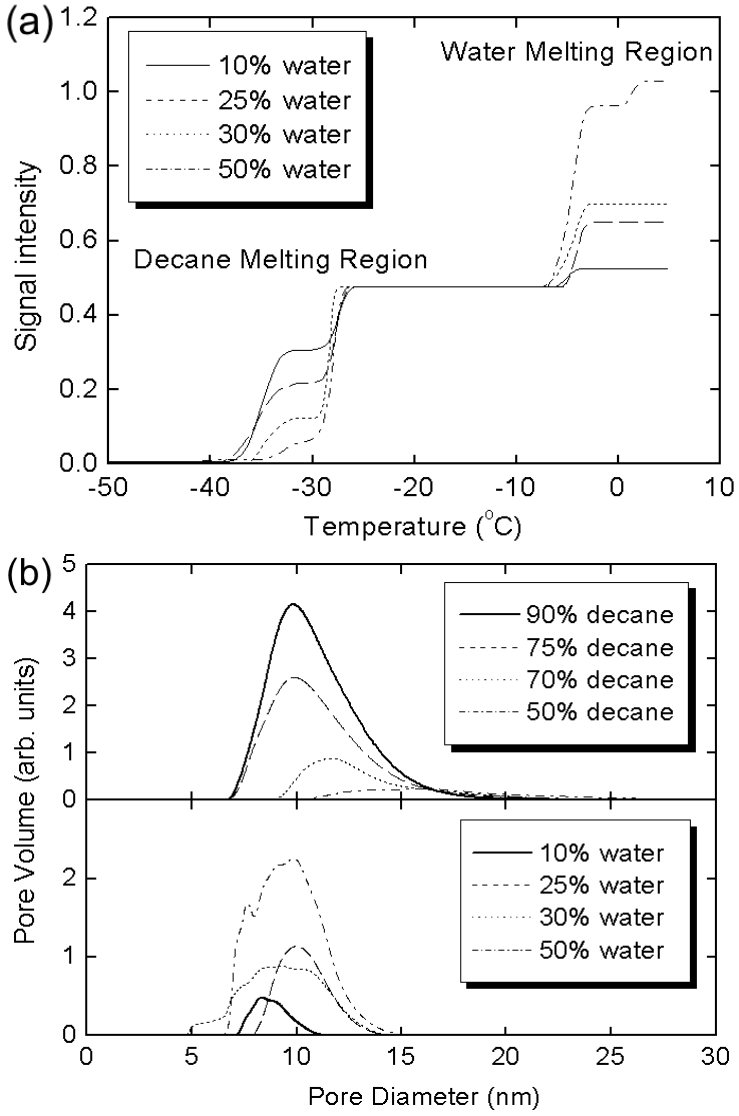

Fig. 9. Results from NMR cryoporometry measurements of water and decane at various ratios in 10 nm median pore diameter silica. (a) Melting curves distinctly showing the separate decane and water fractions. (b) Pore size distributions obtained from data shown in (a) for the decane (top) and water (bottom). As the fraction of water increases, the decane is displaced from the smallest pores first. Graphs reproduced with permission from the American Institute of Physics (Alnaimi et al., 2004).

1985; Prado et al., 1997). The ability to image porosity has been considered by Coussot (Coussot, 1998).

Demonstrations of this technique were published by Strange and Webber (Strange and Webber, 1997), who carefully constructed a set of sol-gel silica phantoms. A one-dimensional phantom was constructed from three sol-gel silicas of pore diameter 6, 14 and 50 nm, separated by spacers. Profiles along the axis of the sample were obtained as a function of temperature, see figure

10. A pore size distribution was obtained for each point in the profile. These measurements were obtained on a permanent magnet operating at 21.5 MHz for ^{1}H. To extend the method to two dimensions a horizontal bore superconducting magnet was utilised. A phantom consisting of four tubes of silica gel with median pore diameters 4, 6, 14, and 20 nm was imaged in cross-section as a function of temperature and pore size distributions were obtained for each pixel in the image; see figure 11. Another phantom was imaged in three dimensions on the same spectrometer; this phantom consisted of a column surrounded by a ring, the two parts having median pore diameters of 6 and 50 nm respectively. By obtaining images at different temperatures, the two regions of silica-gel could be distinguished easily; see figure 12. If enough images were acquired as a function of temperature, it would be possible to obtain pore size distributions on a voxel-by-voxel basis.

7.4 Novel absorbates

Aksnes and Kimtys have compared NMR cryoporometry data for benzene (using ^{1}H NMR) and deuterated benzene (using ^{2}H NMR) in porous glass (Aksnes and Kimtys, 2004). Both absorbates were determined to have the same melting point depression constant of k_{GT} = 88 K nm. In a more recent work by the same authors (Kimtys and Aksnes, 2007) deuterated benzene and cyclohexane were studied in CPG samples by ^{2}H NMR. For benzene-d_6, k_{GT} = 92 K nm with an echo time of 2τ = 1.2 ms (in good agreement with the earlier study); for cyclohexane-d_{12}, k_{GT} = 144 K nm with an echo time of 2τ = 48 . The melting point depressions were found to be equal to the ^{1}H NMR measurements on standard benzene and cyclohexane in the same samples within experimental error. This indicated that there is negligible effect on the proton NMR cryoporometry measurements due to signal originating from physisorbed water and silonal protons on the surface of the glass. The phase transitions of deuterated water in confinement have been studied by neutron diffraction (Dore et al., 2002).

Inorganic salt hydrates can be used as the absorbate in NMR cryoporometry measurements. Zinc nitrate hexahydrate, $Zn(NO_3).6H_2O$, in CPG was determined to have a melting point depression constant k_{GT} = 116 K nm (Vargas-Florencia et al., 2006). Whilst this value is similar to that of organics like benzene and cyclohexane, the hydrophilic nature of the salt makes it easier to imbibe in some porous samples where water would conventionally be used. The authors also noted the salts appeared to shrink on freezing, unlike water, potentially offering another advantage in that the freezing process would not damage delicate pore structures.

The freezing and melting of gallium (Borisov et al., 1997, 1999) and mercury

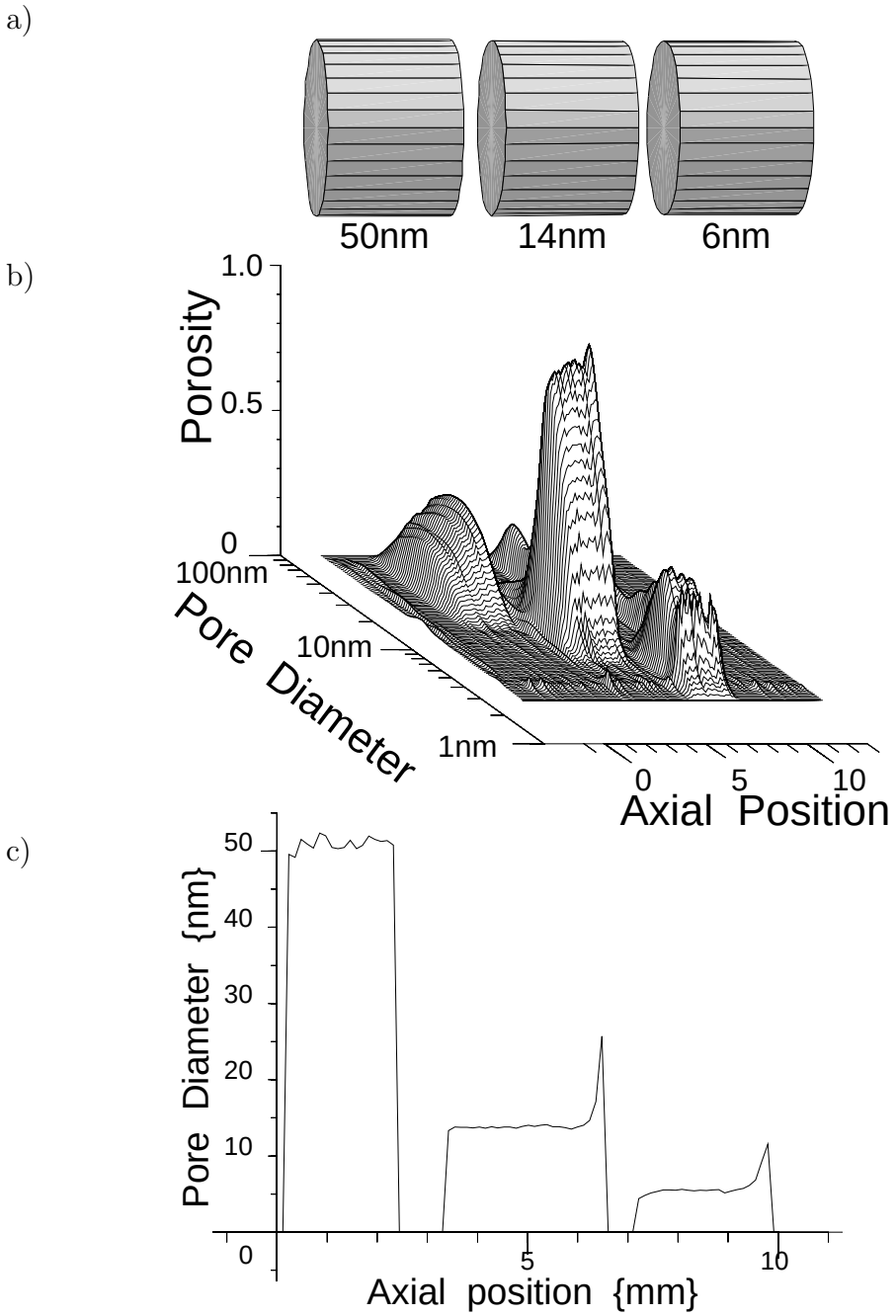

Fig. 10. Spatially resolved pore size distributions from a one-dimensional silica phantom (a) consisting of three regions having median pore diameters of 50, 14, and 6 nm respectively. (b) Profile showing variation of median pore size across the sample. (c) Pore size distributions determined for each point in the profile. Figure reproduced with permission from the Institute of Physics (Strange and Webber, 1997).

a)

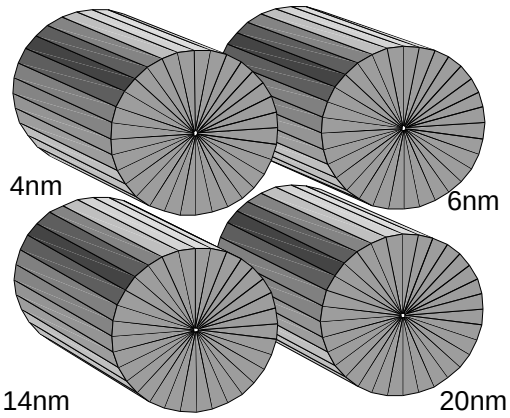

b)

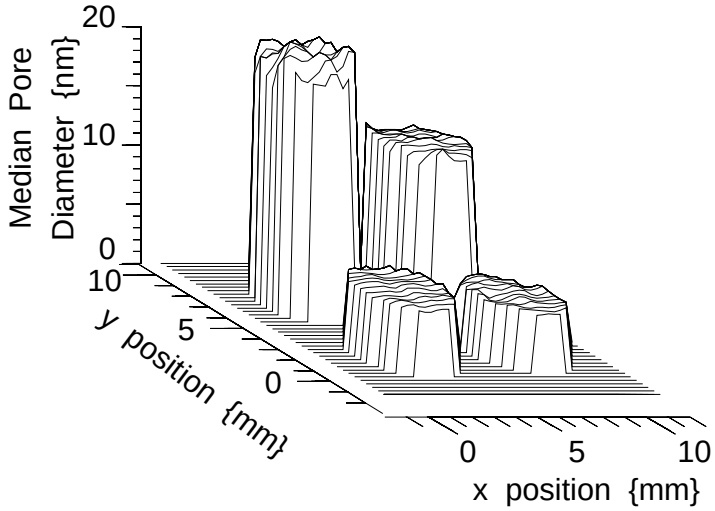

c)

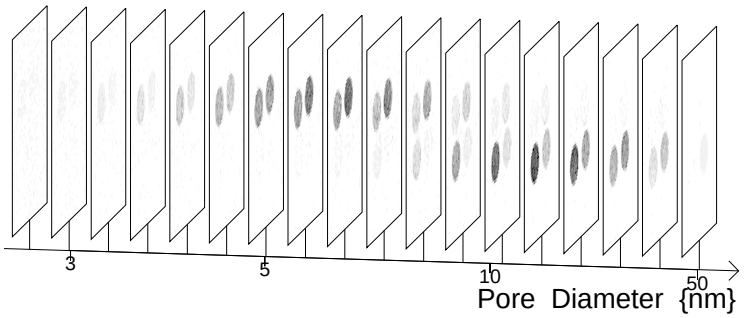

Fig. 11. Spatially resolved NMR cryoporometry measurement of a two-dimensional phantom (a) consisting of silica gels with median pore diameters 4, 6, 14, and 20 nm. (b) Median pore diameters determined as a function of position across the phantom. (c) Pore size distributions determined for each pixel in the cross-section. Figure reproduced with permission from the Institute of Physics (Strange and Webber, 1997).

(Borisov et al., 1998) in porous glass has been studied by ^{71}Ga and ^{199}Hg NMR respectively (Michel et al., 1999). A significant hysteresis was observed between the freezing and melting cycles for both metals. The mercury exhibited broadened phase transitions (Kumzerov et al., 1995) and the melting / freez-

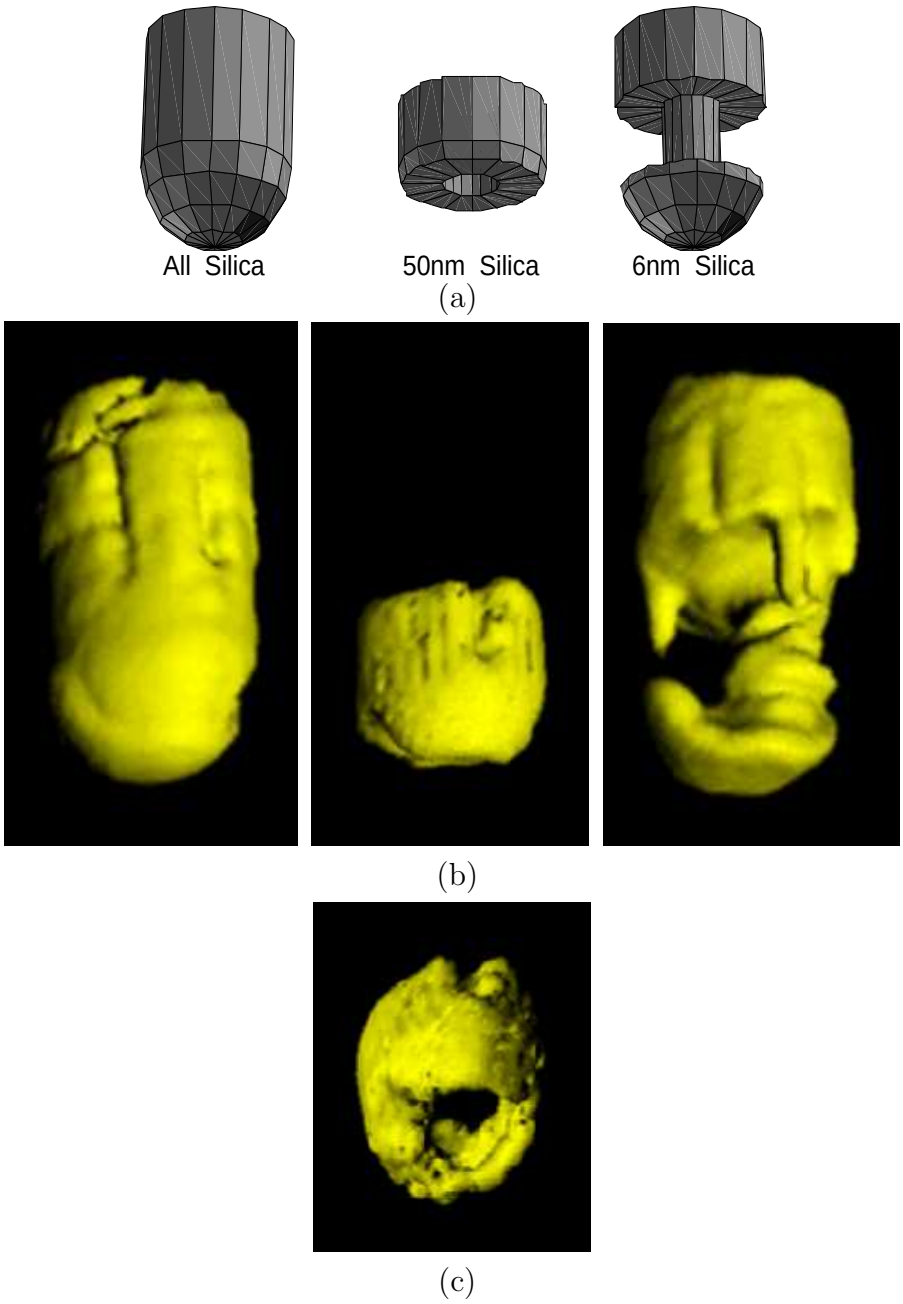

Fig. 12. Spatially resolved NMR cryoporometry measurement of a three-dimensional phantom constructed from 6 and 50 nm median pore diameter silica. (a) The intended shape of the different regions; (b) horizontal views of the volumes rendered from 3D MRI data; and (c) the vertical view of the 50 nm silica volume clearly showing the hollow centre. Figure reproduced with permission from the Institute of Physics (Strange and Webber, 1997).

ing temperatures were dependent on pore size. The gallium appeared to exhibit a freezing point depression determined by the confining pore size, whereas the melting phase transition was considerably narrower and did not appear to reflect the pore size distribution. The NMR Knight shift of the confined metal

suggested it had entered an unusual liquid state (Borisov et al., 1997) and the crystal appeared to have several possible structural phases (Borisov et al., 1999). On some occasions the freezing of the gallium and the mercury was seen to be an irreversible process.

Telkki *et al.* have used ^{130}Xe NMR to measure pore size distributions by dissolving xenon gas in acetonitrile absorbed in silica gels (Telkki et al., 2005b). The behaviour of the xenon was observed as the acetonitrile was frozen. A number of spectral lines were recorded in the ^{130}Xe spectra and these were associated with xenon in different environments. Two of the peaks represented xenon in the bulk and confined liquid acetonitrile and these vanished as the absorbate froze. The difference in intensity or chemical shift of these two peaks could be used to provide the pore size, akin to the method of NMR cryoporometry. Another xenon peak appeared below the depressed melting point of the confined acetonitrile and this was related to free xenon gas trapped in cavities within the porous matrix. The chemical shift of this peak was related to the nominal pore size and so the lineshape of this signal provided a representation of the pore size distribution. ^{1}H NMR cryoporometry on the acetonitrile showed the presence of the dissolved xenon additionally decreased the melting point, altering the pore size distribution obtained (Telkki et al., 2005a). When xenon was dissolved in absorbed cyclohexane, the peak corresponding to xenon trapped in small pockets was not visible, suggesting the solid cyclohexane filled the entire pore structure. Therefore the ^{130}Xe NMR spectra also contained information on the behaviour of the absorbate in confinement. This technique has been applied to the study of liquid crystal in controlled pore glass (Tallavaara et al., 2006).

8 Applications

8.1 Engineering and construction materials

8.1.1 Cement and concrete

The ability to probe the pore structures of cement based materials is of great interest to the engineering community. When cement hydrates it forms a porous structure of Calcium Silicate Hydrate (CSH) that exists in two phases known as the finer and coarser products. These are thought to be laminar structures with characteristic length scales corresponding to the space between the solid hydrate particles. The mean separation of the particles in the finer and coarser products are thought to be on the order of 1.4 nm and 10 – 30 nm respectively, an interpretation supported by NMR relaxometry studies (Monteilhet et al., 2006). NMR cryoporometry is a suitable probe of the ce-

ment microstructure but is less well suited to measuring the larger capillary pores, formed by chemical shrinkage during the hydration process, generally having pore diameters > 150 nm. Unless otherwise stated all the experiments discussed here were conducted on white (architectural) cement due to the lower paramagnetic ion content. It is believed this cement hydrates in the same way as ordinary Portland cement and the products contain identical porosity.

Cement microstructure has been probed with water as the absorbate on melting (Leventis et al., 2000) and freezing (in Portland cement) (Milia et al., 1998), and with cyclohexane as the absorbate (Filippov and Vartapetyan, 1997). Pore size distributions recorded using NMR cryoporometry and other measurements (MIP, nitrogen gas adsorption) on a drying cement paste were notably different (Bhattacharja et al., 1993). The MIP data showed a considerably greater volume occupied by large porosity (0.05 μm) whereas the NMR cryoporometry data suggested there were significantly more small pores (< 0.01 μm) present. Bhattacharja *et al.* explained this discrepancy by saying the mercury was unable to penetrate the small structures. Additionally the MIP and gas adsorption measurements would be unable to probe any closed porosity that could be observed by NMR. Conversely the NMR cryoporometry measurement could yield erroneous results if the hydration process left the pores only partially saturated with water.

Jehng *et al.* have compared NMR cryoporometry and NMR relaxometry analyses of white cement paste with a water-to-cement (w/c) ratio of 0.43 (Jehng et al., 1996); see figure 13. In both cases the free water in the cement was used as the absorbate. Excellent agreement was observed between the two techniques for the smaller pores, where a bimodal distribution was observed. The characteristic modal pore sizes observed were about 5.4 and 14 nm. The two techniques disagreed about the pore distributions in the large capillary pores, figure 13 (insert). The NMR cryoporometry data tailed off above 0.15 μm whereas the NMR relaxometry data suggested a modal pore size of more than 0.2 μm. Valckenborg *et al.* also compared pore size distributions from NMR cryoporometry and NMR relaxometry of a mortar sample using a combined measurement (Valckenborg et al., 2002). The individual pore size distributions obtained from the two techniques can be seen in figure 14. Whilst both techniques revealed three discrete pore sizes, the authors acknowledged that the NMR cryoporometry results were probably more accurate since they did not rely on *a priori* knowledge of the distribution. Due to the regularisation in the Laplace inversion, the NMR relaxometry peaks were forced to be Gaussian in shape.

By combining results from NMR cryoporometry and DSC thermoporosimetry, variations in heats of fusion and surface tension relative to the bulk constants can be determined. This method was used to analyse cement pastes (Hansen et al., 1997a) where ΔH_f = 749 J g^{-1} and γ_{sl} = 1.3 x 10^{-3} J m^{-1}

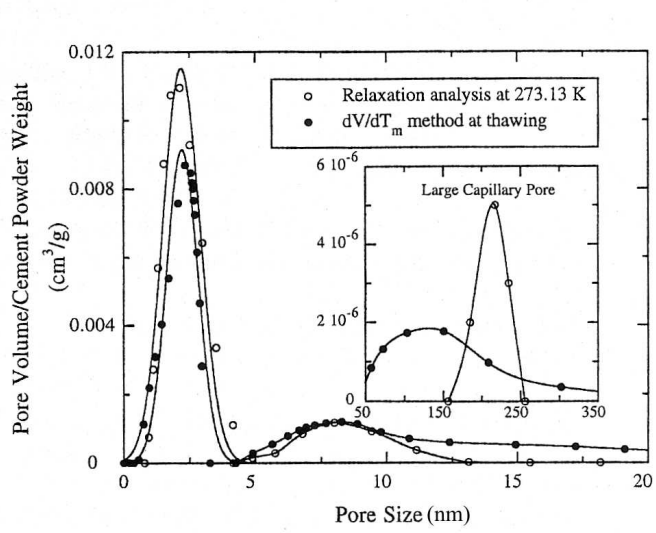

Fig. 13. Pore size distribution for a cement paste determined by NMR cryoporometry (•) and NMR relaxometry (o). Good agreement is shown at small pore sizes but less so in the large capillary pores (insert). The absorbate was water in both cases. Graph reproduced with permission from Elsevier (Jehng et al., 1996).

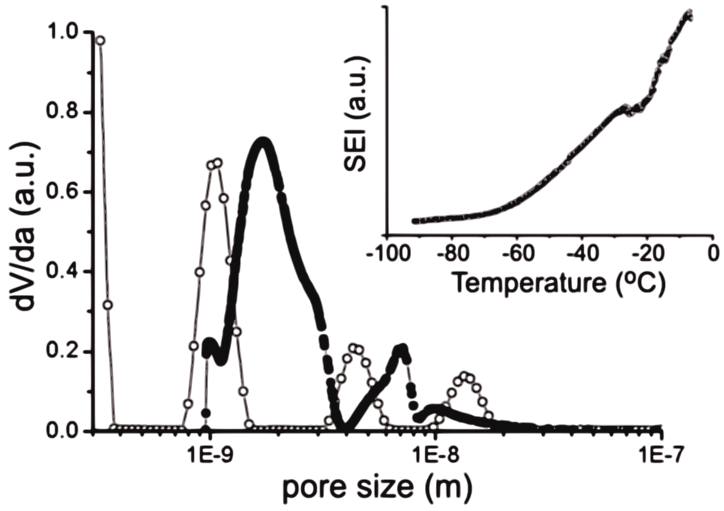

Fig. 14. Pore size distribution for a mortar sample determined by NMR cryoporometry (•) and NMR relaxometry (o). The inset shows the NMR cryoporometry melting curve derived from single echo intensities (SEI). Graph reproduced with permission from the Institute of Physics (Valckenborg et al., 2002).

for the confined water-ice.

Variable temperature MRI images have been used to observe the thawing of water-ice in various cement and concrete samples. Although these studies do not directly provide a pore size distribution they can be used to observe the homogeneity of porosity throughout the sample. The combination of Single Point Imaging (SPI) with T_1 Enhancement (SPRITE) and NMR cryoporometry has

been demonstrated by Prado *et al.* (Prado et al., 1997, 1998a). Subsequently this technique was used to observe frost damage in concrete (Prado et al., 1998b). NMR cryoporometry melting curves were extracted from the profiles to obtain local pore size distributions. This was seen to varying depending on the drying conditions to which the concrete sample had been previously exposed. Additionally, concrete and mortar samples were simultaneously studied to demonstrate the sensitivity of the measurement; see figure 15. This technique was also used to observe the variation in porosity of a partially dried sample (Choi et al., 2000).

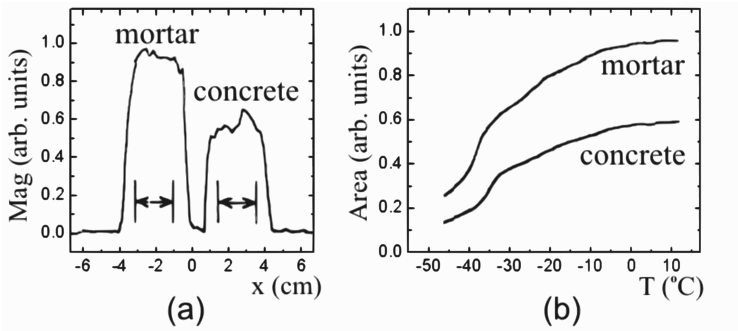

Fig. 15. (a) Spatially resolved profile of mortar and cement samples imaged simultaneously at 12^{o}C. The areas indicated by the arrows were integrated as a function of temperature to create freezing curves (b) for each material. Graphs reproduced with permission from Elsevier (Prado et al., 1998b).

Tritt-Goc *et al.* (Tritt-Goc et al., 2000), Holly *et al.* (Holly et al., 2000), and Boguszyska *et al.* (Boguszynska et al., 2005) have studied the effect of admixtures on the porosity of hydrated cement paste. In the first reference, a combination of T_1 relaxation analysis, SPI, and NMR cryoporometry were used to observe the variation in pore structure of hydrated white cement before and after the addition of 1% superplasticizer (Tritt-Goc et al., 2000). SPI images recorded as the hydrated cement samples were cooled showed the water freezing first in the large macro-pores (cracks) and then in the capillary / coarse product microstructure. The sample containing the superplasticizer was seen to exhibit a much lower total porosity than the untreated cement; see figure 16. Similar experiments were conducted with a nitrate based corrosion inhibitor (Holly et al., 2000). It was demonstrated that the addition of the inhibitor reduced the quantity of fine porosity ($3 < x < 10$ nm) but increased the number of large pores ($x > 10$ nm). The addition of an antifreeze admixture was seen to increase the number of larger pores ($5 < x < 15$ nm) while homogenising the distribution of small pores sizes ($1 < x < 5$ nm) in cement cured at 278 K (Boguszynska et al., 2005). The authors concluded the use of the antifreeze admixture did not detract from the mechanical properties of the cement and it would improve the quality of construction in low temperature environments.

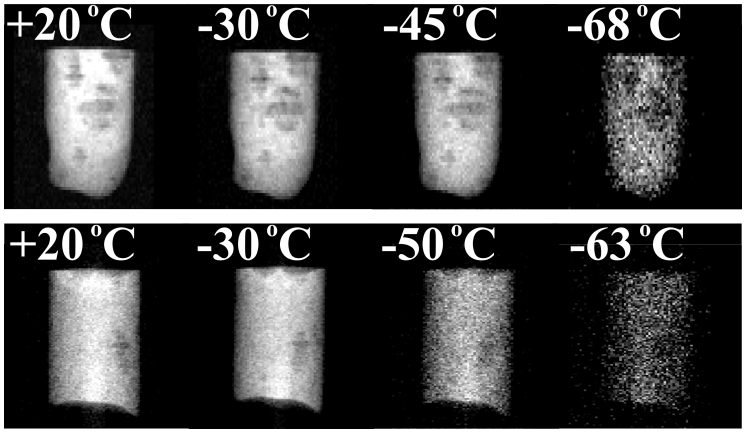

Fig. 16. Single point images showing the freezing of water in cement paste without (top row) and with superplasticizer (bottom row). The inhomogeneous nature of the samples can clearly be seen. The shift in freezing point in between the two samples is also apparent. The grey-scale ranges from black (no signal) to white (maximum signal). Images reproduced with permission from Elsevier (Tritt-Goc et al., 2000).

8.1.2 Carbon products

Coal is a porous form of carbon that has been examined by NMR cryoporometry (Norinaga et al., 1999) and NMR relaxometry analysis (Hayashi et al., 2001; Odintsov et al., 1999). Water absorbed in Yallourn, Beulah Zap, and Illinois #6 coals was used to study the effect of drying on the porosity (Norinaga et al., 1999). An irreversible decrease in porosity was observed following pre-drying and subsequent saturation as a result of porosity collapse and then swelling. This was most pronounced in the Yallourn coal. The pore size distributions indicated the pores with a radius of 2 nm or more had shrunk due to the increase in volume of the solid matrix. A later variable temperature relaxation study on the Yallourn and Beulah Zap coals (Hayashi et al., 2001) suggested the pores were actually slit-shaped and again showed that the pore width decreased with increasing water content due to swelling. The two coals were seen to have characteristic pore dimensions of 2 and 3 nm respectively.

The freezing of water inside single-walled carbon nanotubes (SWCNT) has been studied by variable temperature ^{1}H NMR spectroscopy (Ghosh et al., 2004). The tubes had a diameter of 1.42 nm, smaller than pores generally measured by NMR cryoporometry in silicas. The water was seen to freeze in two stages at temperatures of 242 K and 217 K, corresponding to water in the core of the nanotubes and water at the pore surface respectively. Due to the small diameter of the tubes, the mobile surface layer is a significant fraction of the pore diameter, extending up to 0.3 nm away from the pore wall. These studies supported the simulation work by Koga *et al.* (Koga et al., 2002, 2001). A similar study has since been conducted on H_2O and D_2O in single-walled carbon nanotubes with 1.35 nm diameter (Matsuda et al., 2006). This study also agreed with the simulation and modelling work. Recently variable tem-

perature ^{13}C NMR spectroscopy has been used to study the phase transitions of palmatic acid confined in titanium nanotubes (Tang et al., 2007).

Activated carbons are a special case where depending on preparation the confined liquids may be strongly attracted to the carbon pore surface. Depending on the values of these interactions and on the pore size it is possible to obtain an increase in the melting point of the confined frozen solid, as was experimentally observed by DSC thermoporosimetry with benzene absorbed in activated carbon fibres (Watanabe et al., 1999). These results have been confirmed through comparisons of experimental and simulation data (Radhakrishnan et al., 1999) where both the freezing and melting points were seen to increase above the bulk values. However, such results have yet to be observed using NMR cryoporometry.

Some work has also been done on activated carbons prepared from olive stones (Gonzalez et al., 1994). These carbons have been extensively steam treated, a process that may coat the carbon surface with hydroxyl groups. A number of such carbons have been studied, using both water and cyclohexane as probe liquids. In all cases, standard melting point depressions have been observed for these materials (figure 17a), leading to conventional pore size distributions (figure 17b). Thus, depending on preparation history and surface state, not all activated carbons have the same behaviour.

8.1.3 Rocks and marine sediments

NMR Cryoporometry has been applied to the study of a range of water and oil-bearing porous rocks and marine sediments. It has been noticed that they tend to show an abrupt cut off in porosity at, or just smaller than, 10 nm. They fall into two categories depending on the large pore size distributions: some show a further abrupt reduction in porosity at larger pore diameters (quartz silt, fault rock and kaolin powder), and others exhibit a slower decrease suggesting a fractal distribution of pore sizes (chalk, quartz, shale, ash, and ooze); see figure 18. By adding spatial resolution to NMR cryoporometry measurements of rock core porosity the heterogeneity of the sample can be examined. By imaging the rocks at a selection of temperatures, the distribution of pores over certain lengths scales can be observed; see figure 19.

8.1.4 Wood

The capillary pore structure in wood is generally considered to be on the 1 – 300 nm scale: an ideal range to be probed by NMR cryoporometry. Webber has studied fresh soft and hard wood samples saturated with cyclohexane, see figure 20 (Webber, 2003b). The soft wood was seen to contain a greater open pore volume than the hard wood. In the soft wood, structure was observed

a)

b)

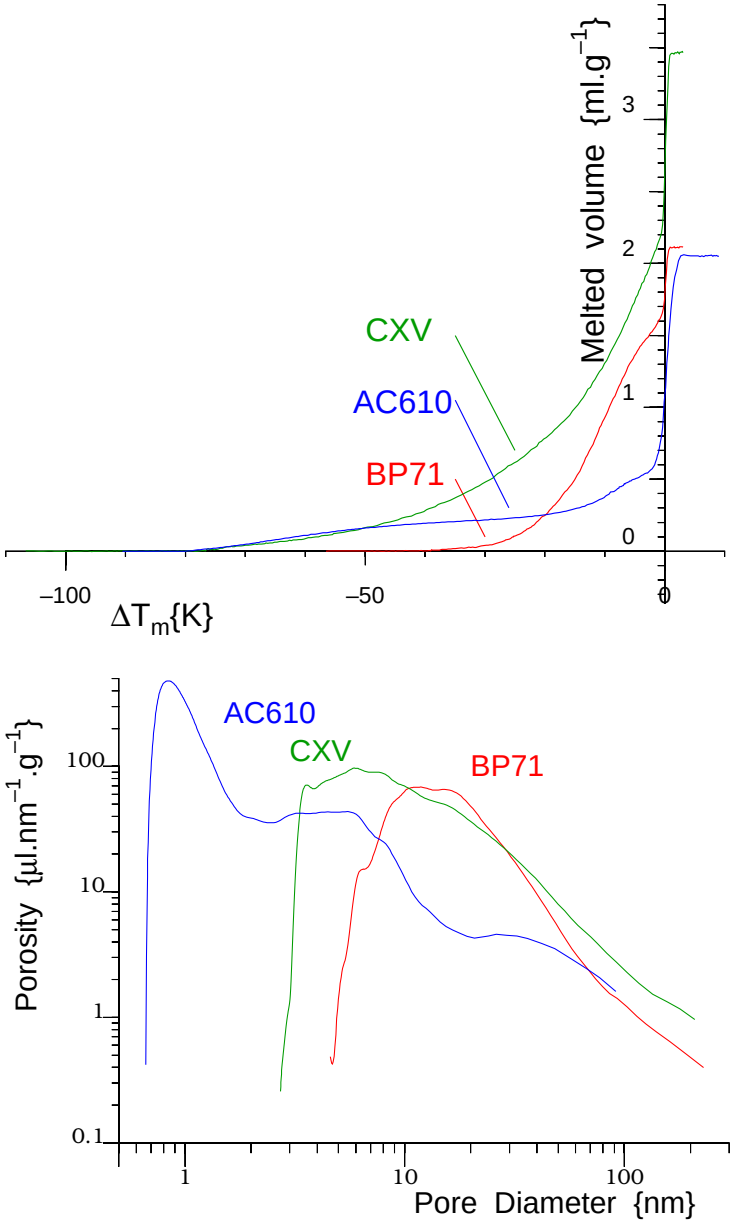

Fig. 17. a) Melting point depressions ΔT_m measured for three olive stone activated carbons, showing the case of water as the probe liquid for sample AC610 and cyclohexane for the larger pore sized samples CXV and BP71. b) Corresponding calculated pore size distributions for the three samples, using the appropriate k_{GT} values as per figure 2. Graphs reproduced with permission from Lab-Tools Ltd.

from 10 nm up to about 10 μm. By contrast, the hard wood appeared to contain fewer small pores, the lower length scale being around 30 nm.

Viel *et al.* used NMR cryoporometry to probe the water fraction trapped in the small pores of an ancient, dehydrated larch wood sample (Viel et al., 2004). A single peak was observed in the pore size distribution, centred on a diameter of 2 nm. In order to probe the much larger open porosity, the sample would need

a)

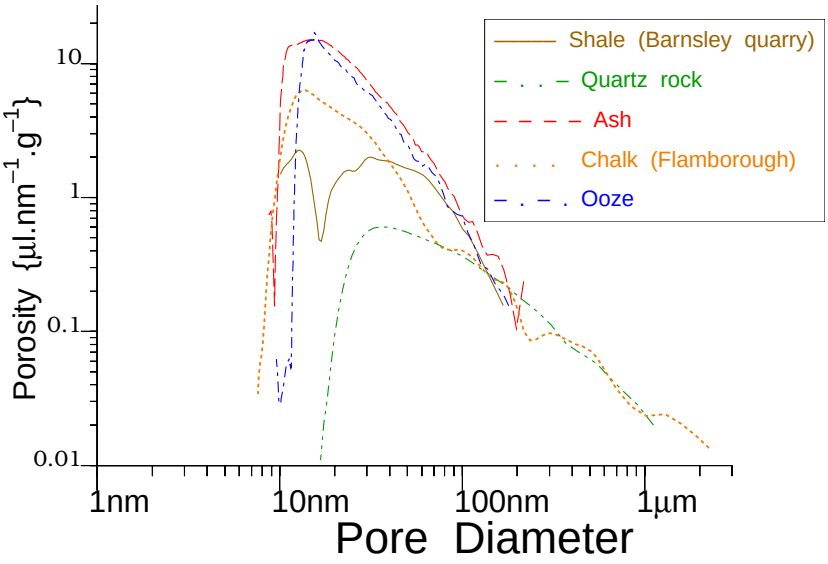

b)

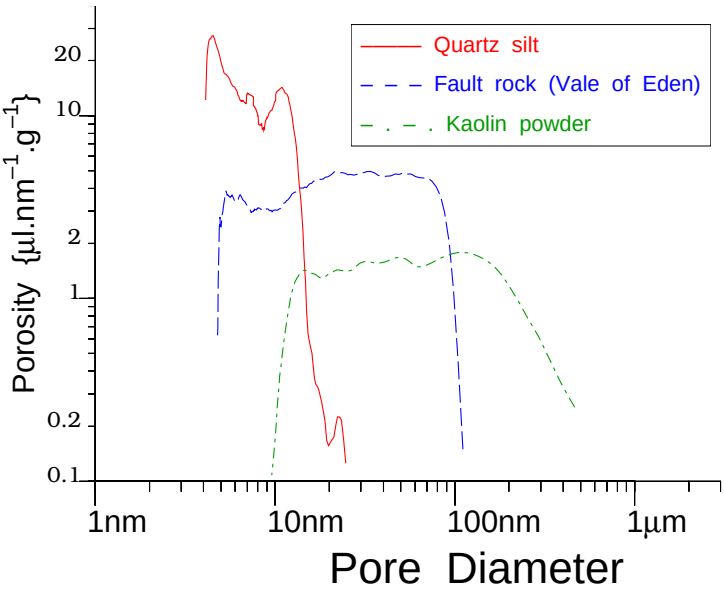

Fig. 18. Pore size distributions for rocks and marine sediments, showing a) fractal behaviour at large pore dimensions, b) non fractal behaviour. Graphs reproduced with permission from Lab-Tools Ltd. and the BMFFFS project (Institute of Petroleum Engineering, Heriot-Watt University).

to be re-hydrated. These measurements were combined with spectroscopic and mobile NMR techniques in an attempt to characterise the condition of wood used in the construction of historic buildings.

8.1.5 Fuel cells

NMR cryoporometry has been used to study the water uptake of Nafion-based membranes, which exhibit similar properties to the membranes present

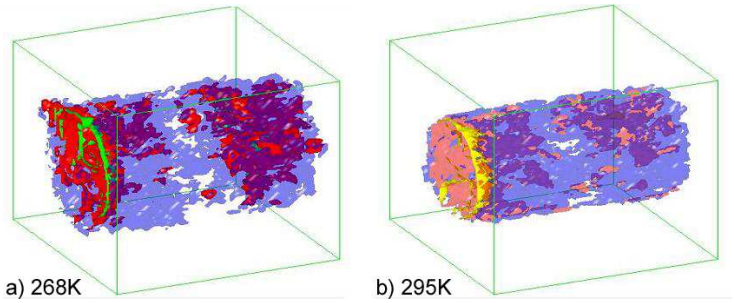

Fig. 19. 3D MRI images obtained for water in a rock core at (a) 268 K and (b) 295 K. Grey-scale intensity relates to water signal (white: no signal; black: maximum signal). Colour-scale (white-blue: little signal; red,green, yellow: strong signal). Images previously displayed in Report to CPMT and presented elsewhere (Strange et al., 2002).

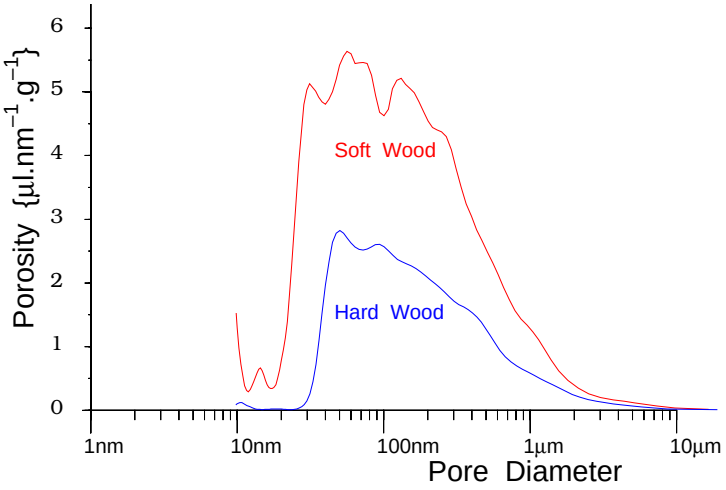

Fig. 20. NMR cryoporometry on soft wood and hard wood samples measured using cyclohexane as the absorbate. Graphs previously presented at MARWINGA project meeting, University of Surrey, 2003 (Webber, 2003b).

in polymer electrolyte membrane fuel cells (PEMFCs) and direct ethanol fuel cells (DEFCs) (Jeon and Kwak, 2007). In this work sulphated β-cyclodextrin (sb-CD) was added to the Nafion to produce proton-conducting membranes. Through a combination of Small Angle X-ray Scattering (SAXS) and ^{1}H NMR cryoporometry measurements, the size of the ionic clusters in the membranes were seen to increase with increasing sb-CD content. As the ionic cluster size increased, the porosity of the clusters also increased, improving the efficiency of water transport across the membrane.

8.2 Gels

^{1}H high-resolution NMR freezing studies of the small water fraction in dried polymethlysiloxane xerogel revealed chemical shifts of σ_H = 1.7, 3.7, and 5

ppm. These were related to weakly associated strongly bound water, strongly associated weakly bound water, and strongly associated strongly bound water respectively (Gun'ko et al., 2007d). NMR cryoporometry studies of the polymethlysiloxane suggested the material has a meso- to macro-scale pore structure with the pores being the spaces between the non-porous primary particles. The exact pore structure varied depending on the degree of agglomeration of the particles.

Characterising aerogels is notoriously difficult since pertabative measurements applying pressure to the structure can alter the porosity (Scherer, 1998). Nevertheless, NMR cryoporometry (with cyclohexane as the absorbate) was successfully used to determine the pore sizes in an aerogel used as a particle collision detector on a low earth orbit spacecraft (Burchell et al., 1999). Since the impact craters of high velocity small particles would be influenced by the density and porosity of the aerogel, it was important to characterise the material. The aerogel was found to have pores in the 40 – 80 nm diameter range with a median pore diameter of 59 nm.

8.3 Fixed bead reactors

Hills and Le Floc'h have studied the behaviour of water and water-ice in beds of porous Sephadex beads containing dextran (Hills and Lefloch, 1994). Variable temperature NMR relaxation analysis measurements were used to identify the behaviour in saturated and unsaturated beds of saturated beads (containing either brine or water). Sephadex beads with smaller pore sizes and a lower concentration of dextran were also explored. A two-phase system was observed to evolve upon freezing of the water inside the beads: water-ice coexisted with unfrozen dextran gel.

Ren *et al.* have proposed a suite of NMR measurements to characterise the porosity of a fixed reactor bed over a large range of length scales (Ren et al., 2003). NMR cryoporometry was just one of the techniques employed: cyclohexane was frozen and then melted in the pores of catalyst pellets. An asymmetric, mono-dispersed pore size distribution was observed with a median pore diameter of 10 nm. This was seen to vary very slightly between the fresh and cooked pellets. ^{130}Xe NMR spectroscopy and NMR relaxometry were also used to analyse the pore structure. NMR diffusion (Callaghan, 1991) and flow propagators (Mitra et al., 1992) were used to investigate the macroscale porosity between the beads in the reactor bed.

8.4 Medical Applications

8.4.1 Bones

NMR cryoporometry has been used, in conjunction with NMR relaxometry, to study the porosity in trabecular bone by Fantazzini *et al.* using cyclohexane as the absorbate (Fantazzini et al., 2001). Pore structure differences were observed in samples from healthy and osteoporotic bones. The bones contained a distribution of pore sizes that extended beyond the limits of NMR cryoporometry. Consequently the signal from the bulk melting (or plastic crystal phase) appeared to overlap with the signal from the pore liquid above a characteristic pore dimension of 40 nm. A large increase in signal was observed corresponding to pores with a mean diameter of approximately 17 nm in the osteoporotic bone, compared to the healthy bone; see figure 21. This confirmed the findings from the NMR relaxometry experiments, whilst able to probe much greater pore length scales, were significantly harder to interpret in terms of accurate pore dimensions. Evans *et al.* highlighted this point, suggesting NMR cryoporometry and gas adsorption as ideal calibration tools for NMR relaxometry (Evans et al., 2005). The wide range of porosities probed by the NMR relaxometry measurement can lead to incorrect analysis if calibrated against limited techniques such as bone histomorphometry (an optical measurement) (Wang and Ni, 2003).

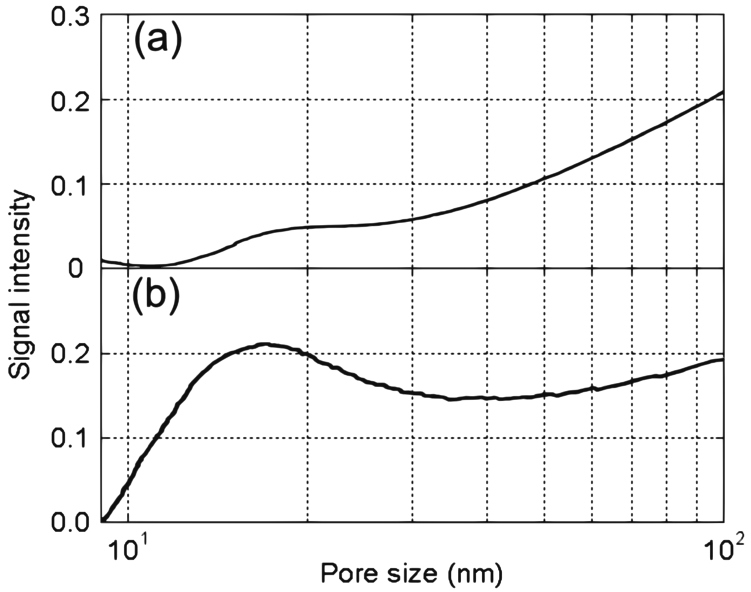

Fig. 21. Pore size distributions obtained from NMR cryoporometry measurements on (a) healthy and (b) osteoporotic bone samples. A significant increase in the porosity can be seen in the osteoporotic bone. Graphs reproduced with permission from Elsevier (Fantazzini et al., 2001).

Gun'ko *et al.* used high-resolution ^{1}H NMR to probe healthy and osteoporotic

human bone (Gun'ko et al., 2006b). As in earlier measurements, a much larger number of mesopores ($2 < x < 50$ nm) and macropores ($x > 50$ nm) were observed in the damaged bone structure. The total porosity and surface area were also found to have increased in the osteoporotic bone. The spectroscopic study allowed the strongly bound and weakly bound water fractions to be identified, as outlined in section 7.2. The ratio of these fractions altered depending on the bond structure and the medium filling the pores. Comparisons were made between the bound water layers when the pores were saturated with air, water, or chloroform-*d*. The chloroform-*d* altered the water distribution since it preferentially filled the larger pores, forcing the water into the smaller structures. Turov *et al.* identified the fractions of weakly and strongly associated water in rat tail bone tissue, and derived the occupied porosities for these two types of water (Turov et al., 2006). The substantial fraction of weakly associated water, $\sigma_H = 1.2 - 1.7$ ppm (much lower than for bulk water), was found to reside in the smallest pores and could only be removed by heating the bone.

8.4.2 Artificial skin

Artificial skins are required to be permeable to water and gasses, but to exclude unwanted organisms. A sample of artificial skin (figure 22) was shown to have a high porosity at a small pore size of 3.9 nm. At larger pore sizes the porosity reduced: the pore volume decreased with increasing pore diameter in such a way as to suggest a fractal arrangement of pores.

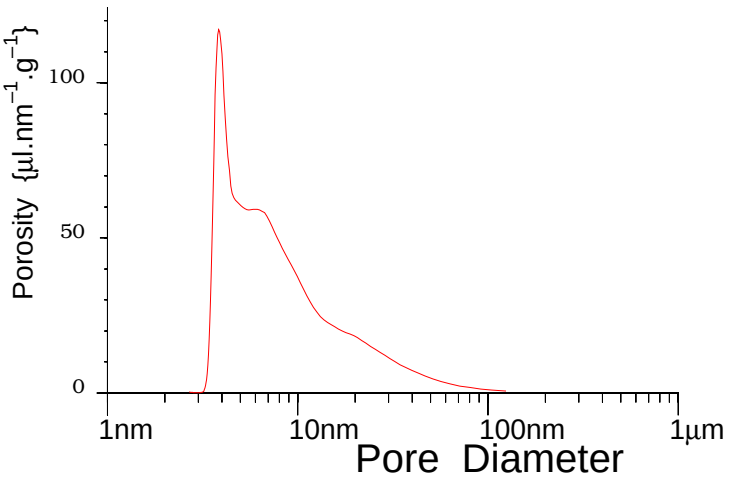

Fig. 22. An example pore size distribution for artificial skin, measured using cyclohexane. The large pore sizes show an approximately fractal distribution, but the peak at 3.7 nm is unusually sharp. Graph reproduced with permission from Lab-Tools Ltd.

8.5 Biological systems

Melanin is deposited in some fungal cell walls and when isolated from the fungus it retains the shape of the cells resulting in hollow spheres called "ghosts". In a study of such melanised ghosts (Eisenman et al., 2005) atomic force, scanning electron, and transmission electron microscopy revealed that the ghosts are covered with roughly spherical granular particles approximately 40 – 130 nm in diameter, and that the melanin is arranged in multiple concentric layers. NMR cryoporometry indicated melanin ghosts contain pores with diameters between 1 – 4 nm, in addition to a small number of pores with diameters near 30 nm. Binding antibodies to the melanin reduced the apparent measured volume of these pores, suggesting a mechanism for their anti-fungal properties.

Yeast cells are stable under dehydration / hydration and freeze / thaw conditions. ^{1}H NMR spectroscopy has been used to study the layer-by-layer freezing of endocellular water in partially hydrated yeast (Turov et al., 2005). The water was found to exist in two states – droplets of bulk-like liquid and two-dimensional surface layers – and the relative volume of these regions was seen to be dependent on the level of hydration. Yeast cells have also been observed to swell under prolonged exposure to water (Gun'ko et al., 2007c). Similar behaviour was observed in wheat seeds in the same work.

The interaction of human plasma fibrinogen and fumed silica in a buffer solution was studied by variable temperature ^{1}H NMR spectroscopy (Rugal et al., 2007; Gun'ko et al., 2007c,a). The proportion of structured water was seen to decrease when the concentration of the fibrinogen and buffer solution increased. This was due to the coagulation of the fibrinogen molecules. Adding fumed silica increased this effect further still as a result of the interaction of the fibrinogen and silica, leading to the formation of densely packed hybrid agglomerates of fibrinogen and silica, and conformational changes in the fibrinogen molecules. The formation of these hybrid agglomerates is important to promoting enhanced blood clotting when fumed silica is incorporated into tourniquet preparations.

8.6 Polymers

8.6.1 Solid structures

Porous structures with length scales suitable for investigation by NMR cryoporometry can be formed by interwoven or layered polymer molecules, such as those in wood fibrils and potato starch (Topgaard and Soderman, 2002). Hansen *et al.* have probed the distribution of water within ideal porous polymer particles (Hansen et al., 2005). The water was seen to occupy four distinct

pore sizes (arbitrarily labeled A, B, C, and D in order of increasing pore size); see figure 23(a). The analysis was performed using a melting point depression constant of $k_{GT} = 84$ K nm and a non-frozen surface layer of 0.5 nm. The four regions were determined to have mean pore diameters of 5, 12.4, 16.4, and 112 nm respectively. Due to experimental limitations the diameter of region A could not be accurately determined by NMR cryoporometry and was confirmed by nitrogen gas adsorption. By combining these results with variable temperature NMR relaxometry measurements, it was possible to determine that pore regions A, B, and D were connected and that regions C and D were connected. However, there did not appear to be any direct connection between regions C and A or B. A model of the polymer pore structure was devised based on these measurements; see figure 23(b).

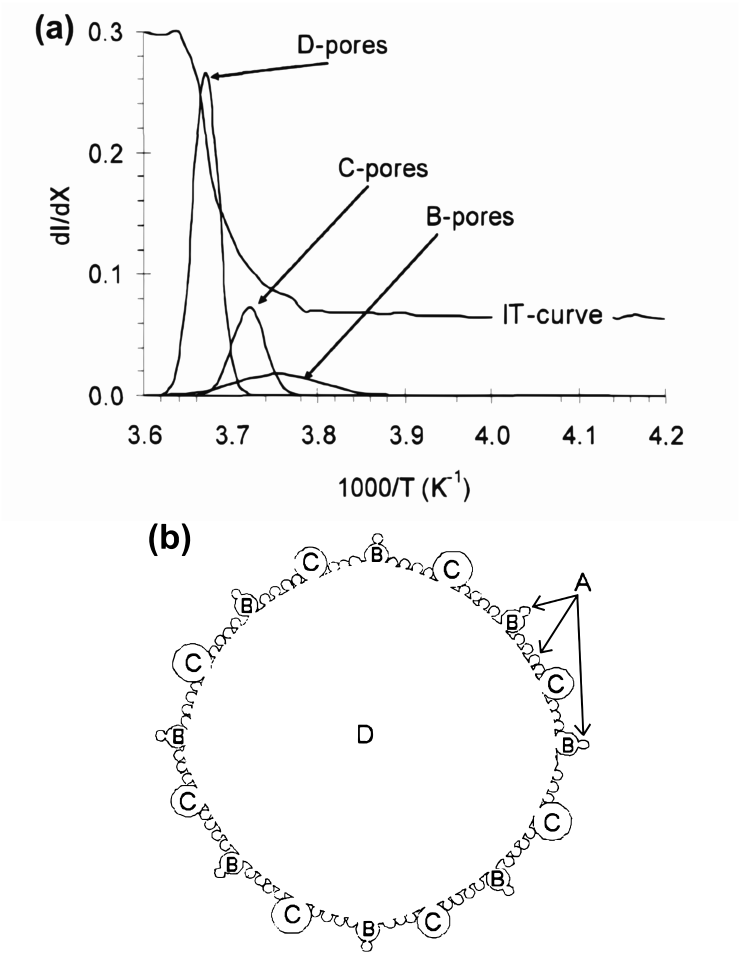

Fig. 23. (a) Pore size distributions obtained from NMR cryoporometry measurements on water in polymer particles. The peaks are associated with the arbitrary labels B, C, and D. The melting curve (IT-curve) is also shown. The smallest pore sizes (A) were not seen in the NMR cryoporometry measurement. (b) A model of the polymer pore structure derived from various measurements. The interconnections between the porosity regions can be seen. Graph and image reproduced with permission from the American Chemical Society (Hansen et al., 2005).

8.6.2 Biodegradable structures

NMR cryoporometry has been applied to the study of biodegradable polymers used in drug delivery (Petrov et al., 2006). Two distinct melting steps were typically observed for water absorbed in the polymer. These steps were associated with water bound in the swollen polymer/gel phase and bulk water. By observing the fraction of water present in the gel phase, the degree of polymer swelling could be deduced. The pore structure revealed by NMR cryoporometry was too small to be resolved by the complimentary scanning electron microscopy (SEM) measurements. The samples with increased nanoscale porosity exhibited a greater degree of swelling and improved drug release characteristics. Although this relationship between drug release and porosity was not conclusively confirmed, the authors acknowledged that NMR cryoporometry was one of the few techniques that allowed reproducible measurements of the smallest pores in water saturated polymeric formulations.

Polyelectrolyte multilayers (PEM) also have applications for drug delivery systems and biosensors. These multilayers are formed by alternately adsorbing anionic and cationic polyelectrolytes onto a surface (Decher et al., 1992). In such applications as encapsulation and controlled release of drugs, the permeability and porosity of the layers is an important factor. Consequently NMR cryoporometry has been used to study the porous structures formed in PEM on silica particles (Chavez and Schonhoff, 2007; Schonhoff et al., 2007). The pores in the silica particles and the PEM were separated by fitting a sum of Gaussian functions to the pore size distribution. Water in the PEM was observed to exist in pores with a characteristic size of 1 nm. The precise mean and standard deviation of the pore size distribution was seen to vary depending on the number of layers in the PEM.

8.6.3 Paper

Paper is a porous cellulose material whose properties are dependent on the quantity of water trapped within the structure. NMR cryoporometry has been used to study paper (Capitani et al., 1996, 1999; Furo and Daicic, 1999; Capitani et al., 2002). In the most recent publication Capitani *et al.* obtained a broad, mono-dispersed pore size distribution with the maximum pore volume occurring for pores of radius 1.4 nm (Capitani et al., 2002). Spectroscopic methods (dipolar filtered ^{13}C MAS and WISE 2D ^{1}H – ^{13}C mapping) were used to measure the distance between the liquid and solid surfaces. These results indicated the pools of water were surrounded by solid cellulose as expected, and that the water pools had dimensions on the order of 1.5 nm in agreement with the NMR cryoporometry result.

8.6.4 Rubber

Standard methods of accessing rubber cross-linking density include swelling the rubbers by absorbing a-polar liquids such as decane until no further extension can be obtained, and then measuring the fractional swelling (Flory and Rehner, 1943; Moore and Watson, 1956). NMR cryoporometry provides an independent method of directly measuring the size of such liquid droplets (and their crystals) within the cross-linked structure of the rubbers (Strange and Webber, 1995; Nedelec et al., 2006). Figure 24 shows the increase in droplet size as a sample of brown rubber is increasingly swollen by adding cyclohexane. This technique has also been used to study black rubber (Strange and Webber, 1995).

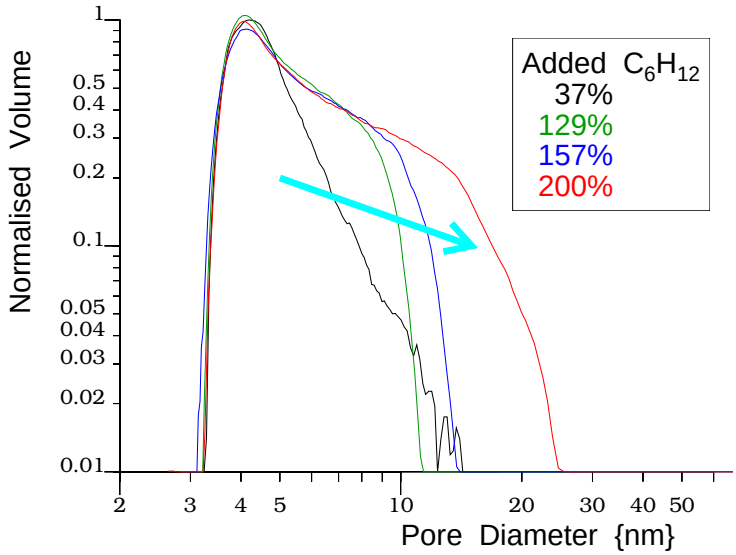

Fig. 24. NMR cryoporometry measurements of the size of cyclohexane droplets in a brown rubber, on swelling of the rubber structure with increasing quantities of cyclohexane (as indicated by the arrow). Graph reproduced with permission from Lab-Tools Ltd.

9 Conclusion

NMR cryoporometry is a non-destructive technique for measuring calibrated pore volume distributions. Although it has not been widely used as a stand alone technique, the ability to provide accurate, reproducible, and unambiguous results has seen NMR cryoporometry become a favoured tool for calibrating NMR relaxometry. NMR cryoporometry has a number of advantages over other equivalent techniques: it can be used to analyse larger and potentially arbitrarily shaped objects (compared to the limited sample size of DSC thermoporosimetry) and is applicable to samples in an aqueous environment (unlike gas adsorption). Ultimately, NMR cryoporometry is at its most potent

when combined with other measurements: NMR relaxometry, spectroscopy, diffusion, and imaging. Together this NMR suite has the potential to probe a great many aspects of porous absorbents and absorbates, from pore morphology, connectivity, heterogeneity, and surface interactions, to the behaviour of binary liquids and partially saturated systems.

In this review we have highlighted the application of NMR cryoporometry to the study of construction materials, polymers, gels, and biological systems including human tissue. It is worth mentioning that NMR cryoporometry has also played a role in many other studies, including the determination of the nature of water-ice (Liu et al., 2006; Dore et al., 2004b; Webber et al., 2007b) and cyclohexane (Dore et al., 2004a) in confinement. Through the numerous measurements of calibrated porous media like silica gels, NMR cryoporometry has helped improve the understanding of pore surface interactions and phenomena including supercooling (Awschalom and Warnock, 1987; Seeley and Seidler, 2001) and the underlying Gibbs-Thomson shift in melting and freezing temperatures (Petrov and Furo, 2006). Combined with powerful new computer modelling simulations (Coasne et al., 2006; Radhakrishnan et al., 2002a) the fundamental physics behind the behaviour of molecules in confinement is slowly being uncovered.

10 Acknowledgements

The authors would like to thank the journal publishers who provided permission to reproduce the figures in this review.

References

Akporiaye, D., Hansen, E. W., Schmidt, R., Stocker, M., Feb 1994. Water-saturated mesoporous MCM-41 systems characterized by H-1-NMR. J. Phys. Chem-US 98 (7), 1926–1928.

Aksnes, D. W., Forland, K., Kimtys, L., 2001. Pore size distribution in mesoporous materials as studied by H-1 NMR. Phys. Chem. Chem. Phys. 3 (15), 3203–3207.

Aksnes, D. W., Gjerdaker, L., Jan 1999. NMR line width, relaxation and diffusion studies of cyclohexane confined in porous silica. J. Mol. Struct. 475 (1), 27–34.

Aksnes, D. W., Kimtys, L., Jan 2004. H-1 and H-2 NMR studies of benzene confined in porous solids: melting point depression and pore size distribution. Solid State Nucl. Mag. 25 (1-3), 146–152.

Alba, M. D., Becerro, A. I., Klinowski, J., Mar 1996. Pore structure analysis

of the mesoporous titanosilicate molecular sieve MCM-41 by H-1 NMR and N-2 sorption. J. Chem. Soc. Faraday 92 (5), 849–854.

Alba-Simionesco, C., Coasne, B., Dosseh, G., Dudziak, G., Gubbins, K. E., Radhakrishnan, R., Sliwinska-Bartkowiak, M., Feb 2006. Effects of confinement on freezing and melting. J. Phys-Condens. Mat. 18 (6), R15–R68.

Allen, S. G., Mallett, M. J. D., Strange, J. H., Feb 2001. Morphology of porous media studied by nuclear magnetic resonance line shapes and spin-echo decays. J. Chem. Phys. 114 (7), 3258–3264.

Allen, S. G., Stephenson, P. C. L., Strange, J. H., May 1997. Morphology of porous media studied by nuclear magnetic resonance. J. Chem. Phys. 106 (18), 7802–7809.

Allen, S. G., Stephenson, P. C. L., Strange, J. H., May 1998. Internal surfaces of porous media studied by nuclear magnetic resonance cryoporometry. J. Chem. Phys. 108 (19), 8195–8198.

Alnaimi, S. M., Mitchell, J., Strange, J. H., Webber, J. B. W., Feb 2004. Binary liquid mixtures in porous solids. J. Chem. Phys. 120 (5), 2075–2077.

Anandan, S., Okazaki, M., Dec 2005. Dynamics, flow motion and nanopore effect of molecules present in the MCM-41 nanopores - an overview. Micropor. Mesopor. Mat. 87 (2), 77–92.

Awschalom, D. D., Warnock, J., May 1987. Supercooled liquids and solids in porous-glass. Phys. Rev. 35 (13), 6779–6785.

Bagshaw, S. A., Hayman, A. R., Jul 2001. Super-microporous silicate molecular sieves. Adv. Mater. 13 (12-13), 1011–1013.

Barrett, E., Joyner, L., Halenda, P., 1951. The determination of pore volume and area distributions in porous substances. J. Am. Chem. Soc. 73, 373–380.

Barrie, P. J., 2000. Characterization of porous media using NMR methods. In: Annual Reports on NMR Spectroscopy, Vol 41. Vol. 41 of Annual Reports on NMR Spectroscopy. Academic Press Inc, San Diego, pp. 265–316.

Bellissentfunel, M. C., Teixeira, J., Bosio, L., Dore, J., Chieux, P., Aug 1986. Spatial correlations in deeply supercooled water. Europhys. Lett. 2 (3), 241–245.

Bellissentfunel, M. C., Teixeira, J., Bosio, L., Dore, J. C., Oct 1989. A structural study of deeply supercooled water. J. Phys-Condens. Mat. 1 (39), 7123–7129.

Beurroies, I., Denoyel, R., Llewellyn, P., Rouquerol, J., Nov 2004. A comparison between melting-solidification and capillary condensation hysteresis in mesoporous materials: application to the interpretation of thermoporometry data. Thermochim. Acta 421 (1-2), 11–18.

Bhattacharja, S., Moukwa, M., Dorazio, F., Jehng, J. Y., Halperin, W. P., Dec 1993. Microstructure determination of cement pastes by NMR and conventional techniques. Adv. Cem. Based Mater. 1 (2), 67–76.

Bloch, F., 1946. Nuclear induction. Phys. Rev. 70, 460–474.

Boguszynska, J., Rachocki, A., Tritt-Goc, J., 2005. Melting behavior of water confined in nanopores of white cement studied by H-1 NMR cryoporometry: Effect of antifreeze additive and temperature. Appl. Magn. Reson. 29 (4),

639–653.
Booth, H. F., Strange, J. H., Feb 1998. Organic nanocrystals: an NMR study of cyclohexane in porous silica. Mol. Phys. 93 (2), 263–269.
Borisov, B. F., Charnaya, E. V., Hoffmann, W. D., Michel, D., Shelyapin, A. V., Kumzerov, Y. A., Apr 1997. Nuclear magnetic resonance and acoustic investigations of the melting-freezing phase transition of gallium in a porous glass. J. Phys-Condens. Mat. 9 (16), 3377–3386.
Borisov, B. F., Charnaya, E. V., Loeser, T., Michel, D., Tien, C., Wur, C. S., Kumzerov, Y. A., Dec 1999. Nuclear magnetic resonance, resistance and acoustic studies of the melting-freezing phase transition of gallium in Vycor glass. J. Phys-Condens. Mat. 11 (50), 10259–10268.
Borisov, B. F., Charnaya, E. V., Plotnikov, P. G., Hoffmann, W. D., Michel, D., Kumzerov, Y. A., Tien, C., Wur, C. S., Sep 1998. Solidification and melting of mercury in a porous glass as studied by NMR and acoustic techniques. Phys. Rev. 58 (9), 5329–5335.
Bosio, L., Teixeira, J., Dore, J. C., Steytler, D. C., Chieux, P., 1983. Neutron-diffraction studies of water 4: The supercooled liquid region (greater-than-or-equal-to-14.5-degrees-c). Mol. Phys. 50 (4), 733–740.
Bosio, L., Teixeira, J., Stanley, H. E., 1981. Enhanced density-fluctuations in supercooled H2O, D2O, and ethanol-water solutions - evidence from small-angle X-ray scattering. Phys. Rev. Lett. 46 (9), 597–600.
Brovchenko, I., Geiger, A., Apr 2002. Water in nanopores in equilibrium with a bulk reservoir - Gibbs ensemble Monte Carlo simulations. J. Mol. Liq. 96-7, 195–206.
Brovchenko, I., Oleinikova, A., Apr 2006. Four phases of amorphous water: Simulations versus experiment. J. Chem. Phys. 124 (16), 12.
Brovchenko, I., Paschek, D., Geiger, A., Sep 2000. Gibbs ensemble simulation of water in spherical cavities. J. Chem. Phys. 113 (12), 5026–5036.
Brownstein, K., Tarr, C., 1979. Importance of classical diffusion in NMR studies of water in biological cells. Phys. Rev. A. 19, 2446–2453.
Brun, M., Lallemand, A., Quinson, J.-F., Eyraud, C., 1977. A new method for the simultaneous determination of the size and the shape of pores: The Thermoporometry. Thermochim. Acta 21, 59–88.
Brunauer, S., Emmett, P., Teller, E., 1938. Adsorption of gases in multimolecular layers. J. Am. Chem. Soc. 60, 309–319.
Bucci, C., Fieschi, R., 1964. Ionic thermoconductivity. method for the investigation of polarization in insulators. Phys. Rev. Lett. 12 (1), 16.
Burchell, M. J., Thomson, R., Yano, H., Jan-Feb 1999. Capture of hypervelocity particles in aerogel: in ground laboratory and low earth orbit. Planet. Space Sci. 47 (1-2), 189–204.
Butler, J. P., Reeds, J. A., Dawson, S. V., 1981. Estimating solutions of 1st kind integral-equations with nonnegative constraints and optimal smoothing. Siam J. Numer. Anal. 18 (3), 381–397.
Callaghan, P. T., 1991. Principles of Nuclear Magnetic Resonance microscopy. Clarendon, Oxford.

Capitani, D., Emanuele, M. C., Bella, J., Segre, A. L., Attanasio, D., Focher, B., Capretti, G., Sep 1999. H-1 NMR relaxation study of cellulose and water interaction in paper. Tappi J. 82 (9), 117–124.

Capitani, D., Proietti, N., Ziarelli, F., Segre, A. L., Jul 2002. NMR study of water-filled pores in one of the most widely used polymeric material: The paper. Macromolecules 35 (14), 5536–5543.

Capitani, D., Segre, A. L., Attanasio, D., Blicharska, B., Focher, B., Capretti, G., Jun 1996. H-1 NMR relaxation study of paper as a system of cellulose and water. Tappi J. 79 (6), 113–122.

Carr, H., Purcell, E., 1954. Effects of diffusion on free precession in NMR experiments. Phys. Rev. 94, 630–638.

Chavez, F. V., Schonhoff, M., Mar 2007. Pore size distributions in polyelectrolyte multilayers determined by nuclear magnetic resonance cryoporometry. J. Chem. Phys. 126 (10), 7.

Chezeau, J., Strange, J., June 1979. Diffusion in molecular-crystals. Phys. Rep. 53 (1), 1–92.

Choi, C., Balcom, B. J., Beyea, S. D., Bremner, T. W., Grattan-Bellew, P. E., Armstrong, R. L., Sep 2000. Spatially resolved pore-size distribution of drying concrete with magnetic resonance imaging. J. Appl. Phys. 88 (6), 3578–3581.

Christenson, H. K., Mar 2001. Confinement effects on freezing and melting. J. Phys-Condens. Mat. 13 (11), R95–R133.

Coasne, B., Jain, S. K., Gubbins, K. E., Sep 2006. Freezing of fluids confined in a disordered nanoporous structure. Phys. Rev. Lett. 97 (10), 4.

Coelingh, M., 1938. Optische onderzoekingen over het vloeistof-dampevenwicht in kapillaire stelsels. Phd, University of Utrecht, Utrecht, Nl.

Cohan, L., 1938. Sorption hysteresis and the vapor pressure of concave surfaces. Journal of the American Chemical Society 60, 433–435.

Coussot, P., Jun-Jul 1998. Pore size NMR imaging. Magn. Reson. Imaging 16 (5-6), 621–623.

Decher, G., Hong, J. D., Schmitt, J., Apr 1992. Build up of ultra-thin multilayer films by a self-assembly process. 3. consecutively alternating adsorption of anionic and cationic polyelectrolytes on charged surfaces. Thin Solid Films 210 (1-2), 831–835.

Defay, R., Prigogine, I., Bellemans, A., Everett, D., 1951 reprinted 1966. Surface tension and adsorption. Longmans, Green, and Co., London.

Denoyel, R., Pellenq, R. J. M., Apr 2002. Simple phenomenological models for phase transitions in a confined geometry. 1: Melting and solidification in a cylindrical pore. Langmuir 18 (7), 2710–2716.

Dominguez, H., Allen, M. P., Evans, R., Jan 1999. Monte Carlo studies of the freezing and condensation transitions of confined fluids. Mol. Phys. 96 (2), 209–229.

Dore, J. C., 2000. Structural studies of water in confined geometry by neutron diffraction. Chem. Phys. 258 (2-3), 327–347.

Dore, J. C., Webber, B., Hartl, M., Behrens, P., Hansen, T., Nov 2002. Neu-

tron diffraction studies of structural phase transformations for water-ice in confined geometry. Physica A. 314 (1-4), 501–507.

Dore, J. C., Webber, B., Strange, J., Farman, H., Descamps, M., Carpentier, L., Feb 2004a. Phase transformations for cyclohexane in mesoporous silicas. Physica A. 333, 10–16.

Dore, J. C., Webber, J. B., Strange, J. H., Jul 2004b. Characterisation of porous solids using small-angle scattering and NMR cryoporometry. Colloid. Surface. 241 (1-3), 191–200.

Dosseh, G., Xia, Y. D., Alba-Simionesco, C., Jul 2003. Cyclohexane and benzene confined in MCM-41 and SBA-15: Confinement effects on freezing and melting. J. Phys. Chem. 107 (26), 6445–6453.

Eisenman, H. C., Nosanchuk, J. D., Webber, J. B. W., Emerson, R. J., Camesano, T. A., Casadevall, A., 2005. Microstructure of cell wall-associated melanin in the human pathogenic fungus cryptococcus neoformans. Biochemistry-US 44, 3683–3693.

Emid, S., Creyghton, J. H. N., 1985. High-resolution NMR imaging in solids. Physica B 128 (1), 81–83.

Evans, L. A., McCutcheon, A. L., Dennis, G. R., Mulley, R. C., Wilson, M. A., Nov 2005. Pore size analysis of fallow deer (dama dama) antler bone. J. Mater. Sci. 40 (21), 5733–5739.

Fantazzini, P., Viola, R., Alnaimi, S. M., Strange, J. H., Apr-May 2001. Combined MR-relaxation and MR-cryoporometry in the study of bone microstructure. Magn. Reson. Imaging 19 (3-4), 481–484.

Feigin, L., Svergun, D., 1987. Structure analysis by small-angle x-ray and neutron scattering. Plenum Press, New York.

Filippov, A. V., Skirda, V. D., Nov-Dec 2000. An investigation of the structure of a porous substance by NMR cryodiffusometry. Colloid J+ 62 (6), 759–764.

Filippov, A. V., Vartapetyan, R. S., Mar-Apr 1997. The NMR study of pore connectivity. Colloid J+ 59 (2), 226–229.

Flory, P., Rehner, J. J., 1943. Chem. Phys. 11, 512.

Furo, I., Daicic, J., Sep 1999. NMR cryoporometry: A novel method for the investigation of the pore structure of paper and paper coatings. Nord. Pulp Paper Res. 14 (3), 221–225.

Gane, P. A. C., Ridgway, C. J., Lehtinen, E., Valiullin, R., Furo, I., Schoelkopf, J., Paulapuro, H., Daicic, J., Nov 2004. Comparison of NMR cryoporometry, mercury intrusion porosimetry, and DSC thermoporosimetry in characterizing pore size distributions of compressed finely ground calcium carbonate structures. Ind. Eng. Chem. Res. 43 (24), 7920–7927.

Gelb, L. D., Gubbins, K. E., Radhakrishnan, R., Sliwinska-Bartkowiak, M., Dec 1999. Phase separation in confined systems. Rep. Prog. Phys. 62 (12), 1573–1659.

Ghosh, S., Ramanathan, K. V., Sood, A. K., Mar 2004. Water at nanoscale confined in single-walled carbon nanotubes studied by NMR. Europhys. Lett. 65 (5), 678–684.

Gibbs, J., 1906 reprinted 1961. The scientific papers of J. Willard Gibbs, new

dover Edition. Vol. 1: Thermodynamics. Dover Publications, Inc., Constable and Co., New York, London.

Gibbs, J., 1928. The collected works of J. Willard Gibbs. Longmans, Green and Co., New York; London.

Gonzalez, M. T., Molinasabio, M., Rodriguezreinoso, F., 1994. Steam activation of olive stone chars, development of porosity. Carbon 32 (8), 1407–1413.

Gregg, S., Sing, K., 1967. Adsorption, surface area and porosity, second edition Edition. Academic Press, London.

Gun'ko, V. M., Galagan, N. P., Grytsenko, I. V., Zarko, V. I., Oranska, O. I., Osaulenko, V. L., Bogatyrev, V. M., Turov, V. V., Dec 2007a. Interaction of unmodified and partially silylated nanosilica with red blood cells. Central European Journal of Chemistry 5 (4), 951–969.

Gun'ko, V. M., Turov, V. V., Barvinchenko, V. N., Bogatyrev, V. M., Turov, A. V., Shulga, O., Stebelska, O. V., Pokrovsky, V. A., Leboda, R., Sukretny, V. G., Nychiporuk, Y. M., Gornikov, Y. I., Chuikov, B. A., Ptushinskii, Y. G., Apr 2006a. Characteristics of interfacial water at nanosilica surface with adsorbed 1,3,5-trihydroxybenzene over wide temperature range. Colloid. Surface. 278 (1-3), 106–122.

Gun'ko, V. M., Turov, V. V., Bogatyrev, V. M., Zarko, V. I., Leboda, R., Goncharuk, E. V., Novza, A. A., Turov, A. V., Chuiko, A. A., Dec 2005. Unusual properties of water at hydrophilic/hydrophobic interfaces. Adv. Colloid Interfac. 118 (1-3), 125–172.

Gun'ko, V. M., Turov, V. V., Leboda, R., Zarko, V. I., Skubiszewska-Zieba, J., Charmas, B., Mar 2007b. Adsorption, NMR, and thermally stimulated depolarization current methods for comparative analysis of heterogeneous solid and soft materials. Langmuir 23 (6), 3184–3192.

Gun'ko, V. M., Turov, V. V., Leboda, R., Zarko, V. I., Skubiszewska-Zieba, J., Charmas, B., Apr 2007c. Comparative analysis of heterogeneous solid and soft materials by adsorption, NMR and thermally stimulated depolarisation current methods. Applied Surface Science 253 (13), 5640–5644.

Gun'ko, V. M., Turov, V. V., Shpilko, A. P., Leboda, R., Jablonski, M., Gorzelak, A., Jagiello-Wojtowicz, E., Nov 2006b. Relationships between characteristics of interfacial water and human bone tissues. Colloid. Surface. 53 (1), 29–36.

Gun'ko, V. M., Turov, V. V., Zarko, V. I., Goncharuk, E. V., Gerashchenko, I., Turova, A. A., Mironyuk, I. F., Leboda, R., Skubiszewska-Zieba, J., Janusz, W., Apr 2007d. Comparative characterization of polymethylsiloxane hydrogel and silylated fumed silica and silica gel. J. Colloid Interf. Sci. 308 (1), 142–156.

Hahn, E. L., 1953. Free nuclear induction. Phys. Today 4 (November), 4–9.

Hahn, E. L., 1956. Spin echoes. Phys. Rev. 80 (4), 580–594.

Hansen, E. W., Fonnum, G., Weng, E., Dec 2005. Pore morphology of porous polymer particles probed by NMR relaxometry and NMR cryoporometry. J. Phys. Chem. 109 (51), 24295–24303.

Hansen, E. W., Gran, H. C., Sellevold, E. J., Aug 1997a. Heat of fusion and

surface tension of solids confined in porous materials derived from a combined use of NMR and calorimetry. J. Phys. Chem. 101 (35), 7027–7032.
Hansen, E. W., Schmidt, R., Stocker, M., Jul 1996a. Pore structure characterization of porous silica by H-1 NMR using water, benzene, and cyclohexane as probe molecules. J. Phys. Chem-US 100 (27), 11396–11401.
Hansen, E. W., Stocker, M., Schmidt, R., Feb 1996b. Low-temperature phase transition of water confined in mesopores probed by NMR. influence on pore size distribution. J. Phys. Chem-US 100 (6), 2195–2200.
Hansen, E. W., Tangstad, E., Myrvold, E., Myrstad, T., Dec 1997b. Pore structure characterization of mesoporous/microporous materials by H-1 NMR using water as a probe molecule. J. Phys. Chem. 101 (50), 10709–10714.
Hayashi, J., Norinaga, K., Kudo, N., Chiba, T., Jul-Aug 2001. Estimation of size and shape of pores in moist coal utilizing sorbed water as a molecular probe. Energ. Fuel. 15 (4), 903–909.
Hills, B. P., Lefloch, G., Jul 1994. NMR-studies of non-freezing water in randomly packed-beds of porous particles. Mol. Phys. 82 (4), 751–763.
Holly, R., Tritt-Goc, J., Pislewski, N., Hansson, C. M., Peemoeller, H., Dec 2000. Magnetic resonance microimaging of pore freezing in cement: Effect of corrosion inhibitor. J. Appl. Phys. 88 (12), 7339–7345.
Jackson, C. L., McKenna, G. B., Dec 1990. The melting behavior of organic materials confined in porous solids. J. Chem. Phys. 93 (12), 9002–9011.
Jehng, J. Y., Sprague, D. T., Halperin, W. P., 1996. Pore structure of hydrating cement paste by magnetic resonance relaxation analysis and freezing. Magn. Reson. Imaging 14 (7-8), 785–791.
Jeon, J. D., Kwak, S. Y., Aug 2007. Ionic cluster size distributions of swollen nafion/sulfated beta-cyclodextrin membranes characterized by nuclear magnetic resonance cryoporometry. Journal of Physical Chemistry B 111 (32), 9437–9443.
Kärger, J., Valiullin, R., Vasenkov, S., Jan 2005. Molecular dynamics under confinement to one dimension: options of measurement and accessible information. New J. Phys. 7, 15.
Khokhlov, A., Valiullin, R., Karger, J., Steinbach, F., Feldhoff, A., Aug 2007. Freezing and melting transitions of liquids in mesopores with ink-bottle geometry. New Journal of Physics 9.
Kimtys, L., Aksnes, D. W., 2007. Analysis of pore size distribution by H-2 NMR. Analyst 132 (2), 148–152.
Koga, K., Gao, G. T., Tanaka, H., Zeng, X. C., Aug 2001. Formation of ordered ice nanotubes inside carbon nanotubes. Nature 412 (6849), 802–805.
Koga, K., Gao, G. T., Tanaka, H., Zeng, X. C., Nov 2002. How does water freeze inside carbon nanotubes? Physica A. 314 (1-4), 462–469.
Koga, K., Zeng, X. C., Tanaka, H., Mar 1998. Effects of confinement on the phase behavior of supercooled water. Chem. Phys. Lett. 285 (3-4), 278–283.
Kumzerov, Y. A., Nabereznov, A. A., Vakhrushev, S. B., Savenko, B. N., Aug 1995. Freezing and melting of mercury in porous-glass. Phys. Rev. 52 (7), 4772–4774.

Leventis, A., Verganelakis, D. A., Halse, M. R., Webber, J. B., Strange, J. H., May 2000. Capillary imbibition and pore characterisation in cement pastes. Transport Porous Med. 39 (2), 143–157.

Liu, E., Dore, J. C., Webber, J. B. W., Khushalani, D., Jahnert, S., Findenegg, G. H., Hansen, T., Nov 2006. Neutron diffraction and NMR relaxation studies of structural variation and phase transformations for water/ice in SBA-15 silica: I. the over-filled case. J. Phys-Condens. Mat. 18 (44), 10009–10028.

Maddox, M. W., Gubbins, K. E., Dec 1997. A molecular simulation study of freezing/melting phenomena for Lennard-Jones methane in cylindrical nanoscale pores. J. Chem. Phys. 107 (22), 9659–9667.

Martin, T., Lefevre, B., Brunel, D., Galarnea, A., Renz, F. D., Fajul, F., Gobi, P. F., Quinson, J. F., Vigier, G., 2002. Dissipative water intrusion in hydrophobic MCM-41 type materials. Chem. Commun. 1, 24–25.

Matsuda, K., Hibi, T., Kadowaki, H., Kataura, H., Maniwa, Y., Aug 2006. Water dynamics inside single-wall carbon nanotubes: NMR observations. Phys. Rev. 74 (7), 4.

Meiboom, S., Gill, D., 1985. Modified spin-echo method for measuring nuclear relaxation times. Rev. Sci. Instrum. 29, 668–691.

Michel, D., Borisov, B. F., Charnaya, E. V., Hoffmann, W. D., Plotnikov, P. G., Kumzerov, Y. A., Jul 1999. Solidification and melting of gallium and mercury in porous glasses as studied by NMR and acoustic techniques. Nanostruct. Mater. 12 (1-4), 515–518.

Milia, F., Fardis, M., Papavassiliou, G., Leventis, A., Jun-Jul 1998. NMR in porous materials. Magn. Reson. Imaging 16 (5-6), 677–678.

Mitchell, J., 2003. A study of the modified behaviour of organic macromolecules in confined geometry. Ph.D. thesis, University of Kent, Canterbury.

Mitchell, J., Stark, S. C., Strange, J. H., Jun 2005. Probing surface interactions by combining NMR cryoporometry and NMR relaxometry. J. Phys. D. Appl. Phys. 38 (12), 1950–1958.

Mitchell, J., Strange, J. H., Oct 2004. An NMR investigation of naphthalene nanostructures. Mol. Phys. 102 (19-20), 1997–2005.

Mitra, P. P., Sen, P. N., Schwartz, L. M., Ledoussal, P., Jun 1992. Diffusion propagator as a probe of the structure of porous-media. Phys. Rev. Lett. 68 (24), 3555–3558.

Monteilhet, L., Korb, J. P., Mitchell, J., McDonald, P. J., Dec 2006. Observation of exchange of micropore water in cement pastes by two-dimensional T-2-T-2 nuclear magnetic resonance relaxometry. Phys. Rev. 74 (6), 9.

Moore, C., Watson, W., 1956. J. Polym. Sci. 19, 237.

Morishige, K., Kawano, K., Mar 1999. Freezing and melting of water in a single cylindrical pore: The pore-size dependence of freezing and melting behavior. J. Chem. Phys. 110 (10), 4867–4872.

Mu, R., Malhotra, V. M., Jul 1992. Geometrically restricted ultrathin (20-nm) film of cyclohexane - a metastable phase. Phys. Rev. 46 (1), 532–535.

Nedelec, J.-M., Grolier, J.-P., Baba, M., Dec. 2006. Thermoporosimetry: A

powerful tool to study the cross-linking in gels networks. J. Sol-Gel Sci. Techn. 40 (2), 191–200.

Newport, R. J., Rainford, B. D., Cywinski, R. (Eds.), 1988. Neutron scattering at a pulsed source. Hilger, Bristol.

Norinaga, K., Hayashi, J., Kudo, N., Chiba, T., Sep-Oct 1999. Evaluation of effect of predrying on the porous structure of water-swollen coal based on the freezing property of pore condensed water. Energ. Fuel. 13 (5), 1058–1066.

Norris, M. O., Strange, J. H., 1969. A nuclear magnetic resonance sample temperature controller using liquid nitrogen injection. J. Phys. E. SciInstrum. 2 (2), 1106–1108.

Odintsov, B. M., Temnikov, A. N., Idiyatullin, Z. S., Kashaev, R. S., Belford, R. L., Ceroke, P. J., Kuriashkin, I. V., Clarkson, R. B., Oct 1999. Particle size effect on transverse NMR relaxation in aqueous char suspensions. Colloid. Surface. 157 (1-3), 177–183.

Overloop, K., van Gerven, L., Feb 1993. Freezing phenomena in adsorbed water as studied by NMR. J. Magn. Reson. Ser. 101 (2), 179–187.

Pearson, R. T., Derbyshire, W., 1974. NMR-studies of water adsorbed on a number of silica surfaces. J. Colloid Interf. Sci. 46 (2), 232–248.

Petrov, O., Furo, I., Jan 2006. Curvature-dependent metastability of the solid phase and the freezing-melting hysteresis in pores. Phys. Rev. 73 (1), 7.

Petrov, O., Furo, I., Schuleit, M., Domanig, R., Plunkett, M., Daicic, J., Feb 2006. Pore size distributions of biodegradable polymer microparticles in aqueous environments measured by NMR cryoporometry. Int. J. Pharm. 309 (1-2), 157–162.

Petrov, O. V., Vargas-Florencia, D., Furo, I., Feb 2007. Surface melting of octamethylcyclotetrasiloxane confined in controlled pore glasses: Curvature effects observed by H-1 NMR. J. Phys. Chem. 111 (7), 1574–1581.

Prado, P. J., Balcom, B. J., Beyea, S. D., Armstrong, R. L., Bremner, T. W., Dec 1997. Concrete thawing studied by single-point ramped imaging. Solid State Nucl. Mag. 10 (1-2), 1–8.

Prado, P. J., Balcom, B. J., Beyea, S. D., Armstrong, R. L., Bremner, T. W., Grattan-Bellew, P. E., Jun-Jul 1998a. Concrete/mortar water phase transition studied by single-point MRI methods. Magn. Reson. Imaging 16 (5-6), 521–523.

Prado, P. J., Balcom, B. J., Beyea, S. D., Bremner, T. W., Armstrong, R. L., Grattan-Bellew, P. E., Feb 1998b. Concrete freeze/thaw as studied by magnetic resonance imaging. Cement Concrete Res. 28 (2), 261–270.

Radhakrishnan, R., Gubbins, K. E., Sliwinska-Bartkowiak, M., Aug 2002a. Existence of a hexatic phase in porous media. Phys. Rev. Lett. 89 (7), 4.

Radhakrishnan, R., Gubbins, K. E., Sliwinska-Bartkowiak, M., Jan 2002b. Global phase diagrams for freezing in porous media. J. Chem. Phys. 116 (3), 1147–1155.

Radhakrishnan, R., Gubbins, K. E., Watanabe, A., Kaneko, K., Nov 1999. Freezing of simple fluids in microporous activated carbon fibers: Comparison

of simulation and experiment. J. Chem. Phys. 111 (19), 9058–9067.
Ren, X. H., Stapf, S., Kuhn, H., Demco, D. E., Blumich, B., Apr-May 2003. Molecular mobility in fixed-bed reactors investigated by multiscale NMR techniques. Magn. Reson. Imaging 21 (3-4), 261–268.
Ritter, H., Drake, L., 1945. Pore-size distribution in porous materials. Industrial and engineering chemistry-analytical edition 17 (12), 782–786.
Roland, U., Renschen, C. P., Lippik, D., Stallmach, F., Holzer, F., Dec 2003. A new fiber optical thermometer and its application for process control in strong electric, magnetic, and electromagnetic fields. Sens. Lett. 1 (1), 93–98.
Rugal, A. A., Gun'ko, V. M., Barvinchenko, V. N., Turov, V. V., Semeshkina, T. V., Zarko, V. I., Mar 2007. Interaction of fibrinogen with nanosilica. Cent. Eur. J. Chem. 5 (1), 32–54.
Samoilenko, A. A., Artemov, D. Y., Sibeldina, L. A., Apr 1988. Formation of sensitive layer in experiments on NMR subsurface imaging of solids. Jetp Lett+ 47 (7), 417–419.
Scherer, G. W., Jul 1998. Characterization of aerogels. Adv. Colloid Interfac. 77, 321–339.
Schmidt, R., Hansen, E. W., Stocker, M., Akporiaye, D., Ellestad, O. H., Apr 1995a. Pore-size determination of MCM-41 mesoporous materials by means of H-1-NMR spectroscopy, N-2 adsorption, and HREM - a preliminary-study. J. Am. Chem. Soc. 117 (14), 4049–4056.
Schmidt, R., Stocker, M., Hansen, E., Akporiaye, D., Ellestad, O. H., Jan 1995b. MCM-41 - a model system for adsorption studies on mesoporous materials. Microporous Mater. 3 (4-5), 443–448.
Schonhoff, M., Ball, V., Bausch, A. R., Dejugnat, C., Delorme, N., Glinel, K., Klitzing, R. V., Steitz, R., Aug 2007. Hydration and internal properties of polyelectrolyte multilayers. Colloids and Surfaces a-Physicochemical and Engineering Aspects 303 (1-2), 14–29.
Seeley, L. H., Seidler, G. T., Jul 2001. Two-dimensional nucleation of ice from supercooled water. Phys. Rev. Lett. 8705 (5), 4.
Seyed-Yazdi, J., Dore, J., Webber, J., Findenegg, G., Hansen, T., submitted. Structural characterisation of water and ice in mesoporous SBA-15 silicas 2: The 'almost-filled' case for 86 å pore diameter.
Seyed-Yazdi, J., Farman, H., Dore, J., Webber, J., Findenegg, G., submitted, b. Structural characterisation of water/ice formation in SBA-15 - 3: The triplet profile.
Sklari, S., Rahiala, H., Stathopoulos, V., Rosenholm, J., Pomonis, P., Nov 2001. The influence of surface acid density on the freezing behavior of water confined in mesoporous MCM-41 solids. Micropor. Mesopor. Mat. 49 (1-3), 1–13.
Sliwinska-Bartkowiak, M., Gras, J., Sikorski, R., Radhakrishnan, R., Gelb, L., Gubbins, K. E., Aug 1999. Phase transitions in pores: Experimental and simulation studies of melting and freezing. Langmuir 15 (18), 6060–6069.
Stapf, S., Kimmich, R., Aug 1995. Molecular-dynamics in confined

monomolecular layers - a field-cycling nuclear-magnetic-resonance relaxometry study of liquids in porous-glass. J. Chem. Phys. 103 (6), 2247–2250.
Stapf, S., Kimmich, R., Aug 1997. Translational mobility in surface induced liquid layers investigated by NMR diffusometry. Chem. Phys. Lett. 275 (3-4), 261–268.
Strange, J. H., Betteridge, L., Mallett, M. J. D., 2002. Characterision of porous media by NMR. In: J., F. (Ed.), NATO ASI series II: Mathematics, Physics and Chemistry. Vol. Magnetic Resonance in Colloid and Interface Science. Kluwer Academic Publishers, Dordrecht.
Strange, J. H., Mitchell, J., 2006. Characterising porous media. In: Dolinšek, J., Vilfan, M., Žumer, S. (Eds.), Novel NMR and EPR techniques. Vol. 684 of Lecture Notes in Physics. Springer, Berlin Heidelberg, pp. 407–430.
Strange, J. H., Mitchell, J., Webber, J. B. W., Apr-May 2003. Pore surface exploration by NMR. Magn. Reson. Imaging 21 (3-4), 221–226.
Strange, J. H., Rahman, M., Smith, E. G., Nov 1993. Characterization of porous solids by NMR. Phys. Rev. Lett. 71 (21), 3589–3591.
Strange, J. H., Webber, J. B., 1995. Characterization of porous solids by nmr. In: 12th Specialized Colloque AMPERE, Dynamics of Partially Disordered Condensed Matter (Corfu, Greece). Athens.
Strange, J. H., Webber, J. B. W., May 1997. Spatially resolved pore size distributions by NMR. Meas. Sci. Technol. 8 (5), 555–561.
Takei, T., Mukasa, K., Kofuji, M., Fuji, M., Watanabe, T., Chikazawa, M., Kanazawa, T., May 2000. Changes in density and surface tension of water in silica pores. Colloid Polym. Sci. 278 (5), 475–480.
Tallavaara, P., Telkki, V. V., Jokisaari, J., Nov 2006. Behavior of a thermotropic nematic liquid crystal confined to controlled pore glasses as studied by Xe-129 NMR spectroscopy. J. Phys. Chem. 110 (43), 21603–21612.
Tang, X. P., Mezick, B. K., Kulkarni, H., Wu, Y., Feb 2007. Elevation of melting temperature for confined palmitic acid inside cylindrical nanopores. J. Phys. Chem. 111 (7), 1507–1510.
Tanner, J. E., Stejskal, E. O., 1968. Restricted self-diffusion of protons in colloidal systems by the pulsed-gradient, spin-echo method. J. Chem. Phys. 49 (4), 1768–1777.
Telkki, V. V., Lounila, J., Jokisaari, J., Jan 2005a. Behavior of acetonitrile confined to mesoporous silica gels as studied by Xe-129 NMR: A novel method for determining the pore sizes. J. Phys. Chem. 109 (2), 757–763.
Telkki, V. V., Lounila, J., Jokisaari, J., Dec 2005b. Determination of pore sizes and volumes of porous materials by Xe-129 NMR of xenon gas dissolved in a medium. J. Phys. Chem. 109 (51), 24343–24351.
Tell, J. L., Maris, H. J., 1983. Specific heats of hydrogen, deuterium, and neon in porous Vycor glass. Phys. Rev. 28 (9), 5122–5125.
Thomson, J., 1849. Theoretical considerations on the effect of pressure in lowering the freezing point of water. Trans. Roy. Soc. Edinburgh xvi (5), 575–580.
Thomson, J., 1862. On crystaliization and liquefaction, as influenced by

stresses tending to change the form in the crystals. Proceedings of the Royal Society 11, 473–481.

Thomson, J., 1888. Applications of dynamics to physics and chemistry. Macmillan and Co., London.

Thomson, W., 1871. On the equilibrium of vapour at a curved surface of liquid. Philosphical Magazine 42 (282), 448–452.

Topgaard, D., Soderman, O., Dec 2002. Self-diffusion of nonfreezing water in porous carbohydrate polymer systems studied with nuclear magnetic resonance. Biophys. J. 83 (6), 3596–3606.

Tritt-Goc, J., Pislewski, N., Koscielski, S., Milia, F., Jun 2000. The influence of the superplasticizer on the hydration and freezing processes in white cement studied by h-1 spin-lattice relaxation time and single point imaging. Cement Concrete Res. 30 (6), 931–936.

Turov, V. V., Gun'ko, V. M., Bogatyrev, V. M., Zarko, V. I., Gorbik, S. P., Pakhlov, E. M., Leboda, R., Shulga, O. V., Chuiko, A. A., Mar 2005. Structured water in partially dehydrated yeast cells and at partially hydrophobized fumed silica surface. J. Colloid Interf. Sci. 283 (2), 329–343.

Turov, V. V., Gun'ko, V. M., Zarko, V. I., Leboda, R., Jablonski, M., Gorzelak, M., Jagiello-Wojtowicz, E., Mar 2006. Weakly and strongly associated nonfreezable water bound in bones. Colloid. Surface. 48 (2), 167–175.

Valckenborg, R. M. E., Pel, L., Kopinga, K., Feb 2002. Combined NMR cryoporometry and relaxometry. J. Phys. D. Appl. Phys. 35 (3), 249–256.

Valiullin, R., Furo, I., Sep 2002a. Low-temperature phase separation of a binary liquid mixture in porous materials studied by cryoporometry and pulsed-field-gradient NMR. Phys. Rev. 66 (3), 10.

Valiullin, R., Furo, I., Aug 2002b. The morphology of coexisting liquid and frozen phases in porous materials as revealed by exchange of nuclear spin magnetization followed by H-1 nuclear magnetic resonance. J. Chem. Phys. 117 (5), 2307–2316.

Valiullin, R., Furo, I., Jan 2002c. Phase separation of a binary liquid mixture in porous media studied by nuclear magnetic resonance cryoporometry. J. Chem. Phys. 116 (3), 1072–1076.

Valiullin, R., Kortunov, P., Kärger, J., Timoshenko, V., Mar 2005. Surface self-diffusion of organic molecules adsorbed in porous silicon. J. Phys. Chem. 109 (12), 5746–5752.

Vargas-Florencia, D., Petrov, O., Furo, I., Mar 2006. Inorganic salt hydrates as cryoporometric probe materials to obtain pore size distribution. J. Phys. Chem. 110 (9), 3867–3870.

Vargas-Florencia, D., Petrov, O. V., Furo, I., Jan 2007. NMR cryoporometry with octamethylcyclotetrasiloxane as a probe liquid. accessing large pores. J. Colloid Interf. Sci. 305 (2), 280–285.

Viel, S., Capitani, D., Proietti, N., Ziarelli, F., Segre, A. L., Jul 2004. NMR spectroscopy applied to the cultural heritage: a preliminary study on ancient wood characterisation. Appl. Phys. A-Mater. 79 (2), 357–361.

Wang, X. D., Ni, Q. W., Mar 2003. Determination of cortical bone porosity and

pore size distribution using a low field pulsed NMR approach. J. Orthopaed. Res. 21 (2), 312–319.

Watanabe, A., Iiyama, T., Kaneko, K., May 1999. Melting temperature elevation of benzene confined in graphitic micropores. Chem. Phys. Lett. 305 (1-2), 71–74.

Watson, A. T., Chang, C. T. P., Nov 1997. Characterizing porous media with NMR methods. Prog. Nucl. Mag. Res. Sp. 31, 343–386.

Webber, B., Dore, J., Nov 2004. Structural and dynamic studies of water in mesoporous silicas using neutron scattering and nuclear magnetic resonance. J. Phys-Condens. Mat. 16 (45), S5449–S5470.

Webber, J. B. W., 2000. Characterising porous media. Ph.D. thesis, University of Kent, Canterbury.

Webber, J. B. W., 2003a. A generalisation of the thermoporisimetry Gibbs-Thomson equation for arbitrary pore geometry. Magn. Reson. Imaging 21 (3-4), 428.

Webber, J. B. W., 2003b. NMR cryoporometry: application to wood composite structures. EC Framework 5 Dissemination Meeting : Magnetic Resonance Imaging of Wood at its Interface with Glue, Coatings and Air.

Webber, J. B. W., Anderson, R., Strange, J. H., Tohidi, B., 2007a. Clathrate formation and dissociation in vapour/water/ice/hydrate systems in SBA-15, Sol-Gel and CPG porous media, as probed by NMR relaxation, novel protocol NMR cryoporometry, neutron scattering and ab-initio quantum-mechanical molecular dynamics simulation. Magn. Reson. Imaging 25 (4), 533–536.

Webber, J. B. W., Dore, J. C., 2008. Neutron Diffraction Cryoporometry – a measurement technique for studying mesoporous materials and the phases of contained liquids and their crystalline forms. Nucl. Instrum. Meth. A. 586, 356–366.

Webber, J. B. W., Dore, J. C., Fischer, H., Vuillard, L., May 1996. Critical scattering by fluid cyclohexane in porous silica. Chem. Phys. Lett. 253 (3-4), 367–371.

Webber, J. B. W., Dore, J. C., Strange, J. H., Anderson, R., Tohidi, B., 2007b. Plastic ice in confined geometry: The evidence from neutron diffraction and NMR relaxation. J. Phys.: Condens. Matter 19, 415117 (12pp).

Webber, J. B. W., Strange, J. H., Dore, J. C., Apr-May 2001. An evaluation of NMR cryoporometry, density measurement and neutron scattering methods of pore characterisation. Magn. Reson. Imaging 19 (3-4), 395–399.

Xie, X. L., Satozawa, M., Kunimori, K., Hayashi, S., Sep 2000. NMR study of pore surface and size in the mesoporous material FSM-16. Micropor. Mesopor. Mat. 39 (1-2), 25–35.

Young, T., 1805. An essay on the cohesion of fluids. Philos. T. Roy. Soc. 95, 65–87.

Young, T., 1855. An essay on the cohesion of fluids. In: Peacock, G. (Ed.), Miscellaneous Works of the late Thomas Young. Vol. 1. John Murray, Albemarle Street, London, Ch. XIX, pp. 418–453.

Zanotti, J. M., Bellissent-Funel, M. C., Chen, S. H., Jul 2005. Experimental evidence of a liquid-liquid transition in interfacial water. Europhys. Lett. 71 (1), 91–97.